Multiple-scattering theory for two-dimensional electron gases in the presence of spin-orbit coupling

Jamie D. Walls,[1,*] Jian Huang,[2] Robert M. Westervelt,[2,3] and Eric J. Heller[1,2]
[1]*Department of Chemistry and Chemical Biology, Harvard University, Cambridge, Massachusetts 02138, USA*
[2]*Department of Physics, Harvard University, Cambridge, Massachusetts 02138, USA*
[3]*Division of Engineering and Applied Sciences, Harvard University, Cambridge, Massachusetts 02138, USA*
(Received 25 July 2005; revised manuscript received 17 November 2005; published 23 January 2006)

In order to model the phase-coherent scattering of electrons in two-dimensional electron gases in the presence of Rashba spin-orbit coupling, a general partial-wave expansion is developed for scattering from a cylindrically symmetric potential. The theory is applied to possible electron flow imaging experiments using a moveable scanning probe microscope tip. In such experiments, it is demonstrated theoretically that the Rashba spin-orbit coupling can give rise to spin interference effects, even for unpolarized electrons at nonzero temperature and no magnetic field.

DOI: 10.1103/PhysRevB.73.035325 PACS number(s): 73.63.−b, 03.65.Nk, 71.70.Ej, 72.25.Rb

I. INTRODUCTION

There has been recent interest[1–3] in utilizing the spin degree of freedom in semiconductor devices, where the charge carrier's spin provides an additional degree of control and flexibility towards developing devices that are faster and more efficient devices than conventional electronic devices. One component of potential "spintronic" devices, the spin transistor proposed by Datta and Das,[4] modulates the current passing through a semiconductor due to the presence of the spin-orbit interaction, which couples the electron's spin with its kinematical motion. Interest in the spin transistor has generated numerous theoretical and experimental investigations into the spin dynamics under the spin-orbit interaction in two-dimensional electron gases (2DEG).

In layered semiconductors devices, the two predominant sources of spin-orbit coupling arise from either structure inversion asymmetry (SIA or Rashba interaction[5]) or bulk inversion asymmetry (BIA or Dresselhaus interaction[6]). The BIA spin-orbit interaction arises from the breaking of inversion symmetry by the inherent asymmetry of the atomic arrangement in the structure and is not very amenable to external manipulation. The Rashba spin-orbit coupling, on the other hand, arises from band bending at the interfaces between semiconductor layers and/or any external electric fields applied to the the device. Unlike the Dresselhaus coupling, the strength of the Rashba coupling can be partially controlled by application of an external electric field[7] and in principle can be made the dominant form of spin-orbit interaction in the 2DEG. Such tunability of the Rashba interaction is ideally suited for applications in spintronic devices, and as such, only the Rashba spin-orbit coupling will be considered in this study.

Numerous studies have been conducted on the diffusive transport of spins in the presence of spin-orbit coupling[8–10] in order to investigate a variety of phenomena, such as the spin Hall effect.[11,12] Most of the studies were conducted up to the first-Born approximation for the scattering from nonmagnetic impurities, and the results were disorder averaged. However, there are many cases where such statistical theories are not warranted. For example, coherent scattering from a fixed set of impurities, which give rise to quantum interference effects induced by multiple-scattering events from the localized impurities, cannot be described by such statistical theories. One method of tackling such problems is multiple scattering theory, which has been routinely used in optical and acoustic scattering and has been proposed as a method for understanding the fringing patterns in recent imaging experiments on electron flow in 2DEG.[13,14] In scattering theory, the effect of a scatterer k can be localized to a point in space at the center of the scatterer $\vec{r}_k$, such that an operator $\hat{T}_k$ can be constructed which generates the scattered wave $\Psi_S(\vec{R})$ from the incident wave $\Phi_{\text{in}}(\vec{R})$ evaluated at the site of the scatterer $\vec{R}=\vec{r}_k$:

$$\Psi(\vec{R}) = \Phi_{\text{in}}(\vec{R}) + \Psi_S(\vec{R}) = \Phi_{\text{in}}(\vec{R}) + [\hat{T}_k(\vec{R},\vec{r})\Phi_{\text{in}}(\vec{r})]_{\vec{r}=\vec{r}_k}. \tag{1}$$

The subscript $\vec{r}=\vec{r}_k$ means to operate $\hat{T}_k(\vec{R},\vec{r})$ upon $\Phi_{\text{in}}(\vec{r})$ and evaluate the result at $\vec{r}=\vec{r}_k$. In the presence of N point scatterers, the total wave function is then given by

$$\Psi(\vec{R}) = \Phi_{\text{in}}(\vec{R}) + \sum_{k=1}^{N} [\hat{T}_k(\vec{R},\vec{r})\Psi(\vec{r})]_{\vec{r}=\vec{r}_k}. \tag{2}$$

Thus the complete wave function can be found if $[\hat{T}_k(\vec{R},\vec{r})\Psi(\vec{r})]_{\vec{r}=\vec{r}_k}$ is known at each scatter k.

In the following article, a multiple-scattering theory in the presence of Rashba spin-orbit coupling in a 2DEG is developed. The general formalism is presented, along with the explicit calculation of the scattering operator $\hat{T}_k$ for a cylindrically symmetric well/barrier, which will be used as a model for impurities in a 2DEG. As an application, the methodology is applied to possible flux measurements for phase-coherent transport in a 2DEG with Rashba spin-orbit interaction in the presence of a scanning probe microscope (SPM)

tip in zero magnetic field. Additional interference effects arise in the flux measurements due to spin interference effects caused by the Rashba coupling.

II. SCATTERING FROM A CYLINDRICALLY SYMMETRIC POTENTIAL: PARTIAL-WAVE EXPANSION

The Hamiltonian for a 2DEG in the presence of the Rashba spin-orbit interaction and impurities is given by

$$\hat{H} = \frac{\hat{p}_X^2}{2m^*} + \frac{\hat{p}_Y^2}{2m^*} - \frac{\alpha}{\hbar}(\hat{p}_Y\hat{\sigma}_X - \hat{p}_X\hat{\sigma}_Y) + V(x,y) = \hat{H}_0 + V(x,y), \tag{3}$$

where $\hat{\sigma}_j$ are the Pauli spin matrices and α is the Rashba spin-orbit coupling constant. The eigenstates and corresponding eigenvalues for the free-particle Hamiltonian with Rashba spin-orbit coupling $\hat{H}_0$, are given by

$$|k(\theta), \pm(\theta)\rangle = |k_Y = k\cos(\theta), k_X = k\sin(\theta)\rangle|\pm(\theta)\rangle \tag{4}$$

$$E_\pm = \frac{\hbar^2 k^2}{2m^*} \mp \alpha k, \tag{5}$$

where

$$\tan(\theta) = \frac{k_X}{k_Y},$$

$$|\pm(\theta)\rangle = \frac{1}{\sqrt{2}}\begin{pmatrix} 1 \\ \pm\exp(-i\theta) \end{pmatrix}, \tag{6}$$

and $k = \sqrt{k_X^2 + k_Y^2}$.

The dispersion relation in Eq. (5) represents two parabolic bands centered upon $k = \pm m^*\alpha/\hbar^2$. For states propagating with their momentum vectors making an angle θ with respect to the $\hat{Y}$ axis and for an energy $E \geqslant 0$, there exists a twofold degeneracy with the degenerate states given by

$$|k_1(\theta), +(\theta)\rangle = |\vec{k}_1(\theta)\rangle\sqrt{\frac{1}{2}}\begin{pmatrix} 1 \\ \exp(-i\theta) \end{pmatrix}, \tag{7}$$

$$|k_2(\theta), -(\theta)\rangle = |\vec{k}_2(\theta)\rangle\sqrt{\frac{1}{2}}\begin{pmatrix} 1 \\ -\exp(-i\theta) \end{pmatrix}, \tag{8}$$

where $\vec{k}_{1(2)} = k_{1(2)}[\cos(\theta)\hat{Y} + \sin(\theta)\hat{X}]$ with

$$k_1 = \frac{m^*\alpha}{\hbar^2} + \sqrt{\left(\frac{m^*\alpha}{\hbar^2}\right)^2 + \frac{2m^*E}{\hbar^2}},$$

$$k_2 = -\frac{m^*\alpha}{\hbar^2} + \sqrt{\left(\frac{m^*\alpha}{\hbar^2}\right)^2 + \frac{2m^*E}{\hbar^2}}. \tag{9}$$

The states $|k_1(\theta), +(\theta)\rangle$ and $|k_2(\theta), -(\theta)\rangle$ represent plane-wave states whose spin states are quantized in the plane, perpendicular to the momentum direction.

In polar coordinates, which are useful when considering scattering from a localized, cylindrically symmetric potential, $\hat{H}_0$ can be written as

$$\hat{H}_0 = -\frac{\hbar^2}{2m^*}\left(\frac{\partial^2}{\partial r^2} + \frac{1}{r}\frac{\partial}{\partial r} + \frac{1}{r^2}\frac{\partial^2}{\partial\theta^2}\right) + i\alpha\begin{pmatrix} 0 & \exp(i\theta)\left(\frac{\partial}{\partial r} + \frac{i}{r}\frac{\partial}{\partial\theta}\right) \\ \exp(-i\theta)\left(\frac{\partial}{\partial r} - \frac{i}{r}\frac{\partial}{\partial\theta}\right) & 0 \end{pmatrix}. \tag{10}$$

The eigenstates of $\hat{H}_0$ which represent states propagating outward from or towards a particular origin $\vec{r}_i$ can be written as

$$\langle\vec{R}|\chi^\pm_{l,\uparrow,E}\rangle = \chi^\pm_{l,\uparrow}(\vec{R},E) = \exp(il\theta)\frac{\sqrt{k_1}}{2\sqrt{2}}\begin{pmatrix} H_l^\pm(k_1|\vec{R}-\vec{r}_i|) \\ -iH_{l-1}^\pm(k_1|\vec{R}-\vec{r}_i|)\exp(-i\theta) \end{pmatrix},$$

$$\langle\vec{R}|\chi^\pm_{l,\downarrow,E}\rangle = \chi^\pm_{l,\downarrow}(\vec{R},E) = \exp(il\theta)\frac{\sqrt{k_2}}{2\sqrt{2}}\begin{pmatrix} H_l^\pm(k_2|\vec{R}-\vec{r}_i|) \\ iH_{l-1}^\pm(k_2|\vec{R}-\vec{r}_i|)\exp(-i\theta) \end{pmatrix}, \tag{11}$$

where $H_l^\pm(z)$ are Hankel functions given by $H_l^\pm(z) = J_l(z) \pm iY_l(z)$, and k_1 and k_2 are given in Eq. (9). A similar solution to Eq. (10) for a cylindrical well has been given before.[15,16] The states $\chi^\pm_{l,\uparrow(\downarrow)}(\vec{R},E)$ satisfy a flux orthogonality condition through a circular surface surrounding the origin, $\vec{r}_i$, which is given by

$$\frac{1}{2}\int_0^{2\pi}\langle\chi^\pm_{l,a,E}|[|\vec{R}(\theta)\rangle\langle\vec{R}(\theta)|\hat{\vec{J}} + \hat{\vec{J}}|\vec{R}(\theta)\rangle\langle\vec{R}(\theta)|]|\chi^\pm_{m,b,E}\rangle\cdot\vec{R}(\theta)d\theta = \frac{\hbar\bar{k}}{m^*}\delta_{l,m}\delta_{a,b}, \tag{12}$$

where the current operator $\hat{J}$ is given by

$$\hat{\vec{J}} = \hat{J}_X\hat{X} + \hat{J}_Y\hat{Y} = \left(\frac{\hat{p}_X}{m^*} + \frac{\alpha}{\hbar}\hat{\sigma}_Y\right)\hat{X} + \left(\frac{\hat{p}_Y}{m^*} - \frac{\alpha}{\hbar}\hat{\sigma}_X\right)\hat{Y}. \tag{13}$$

The states in Eq. (11) can be used to generate the scattering operator $\hat{T}_k$ [Eq. (1)] for scattering in the presence of Rashba spin-orbit coupling. The following treatment follows closely a previous treatment for constructing $\hat{T}_k$ in the absence of spin-orbit coupling.[17] We will begin by solving the Schrödinger equation for an eigenstate of $\hat{H}_0$ [Eq. (3)] incident upon a cylindrically symmetric potential centered at $\vec{r}_k$, $V_k(\vec{r})$, as shown in Fig. 1. $V_k(\vec{r})$ is given by

$$V_k(\vec{r}) = \begin{cases} V_0 & \text{for } |\vec{r}-\vec{r}_k| \leqslant a, \\ 0 & \text{for } |\vec{r}-\vec{r}_k| > a, \end{cases} \tag{14}$$

where a is the radius of the scattering potential. Consider the case of an incident wave propagating with momentum $\vec{k}_\pm = k_\pm[\cos(\theta_0)\hat{Y} + \sin(\theta_0)\hat{X}]$, where $\pm$ denotes a particular eigenstate of H_0 $[|\vec{k}_+(\theta_0), +(\theta_0)\rangle = |\vec{k}_1(\theta_0), +(\theta_0)\rangle$ and

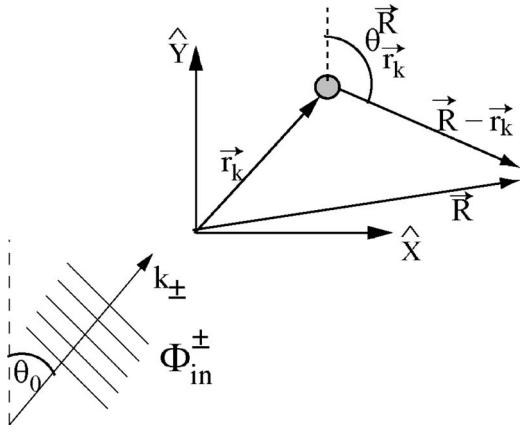

FIG. 1. Scattering of an incident plane wave $\Phi_{\text{in}}^{\pm}(\vec{R})$ [Eq. (15)] from a potential located at $\vec{r}_k$, $V_k(\vec{R})$ [Eq. (14)]. The various angles and vectors used in Eqs. (15) and (16) are illustrated.

$|\vec{k}_-(\theta_0),-(\theta_0)\rangle=|\vec{k}_2(\theta_0),-(\theta_0)\rangle$ given in Eqs. (7) and (8)]. The incident wave function $\Phi_{\text{in}}^{\pm}(\vec{R})$ written in a coordinate system centered about the scatterer at $\vec{r}_k$ is given by

$$\begin{aligned}\Phi_{\text{in}}^{\pm}(\vec{R}) &= \frac{1}{\sqrt{2}}\exp(i\vec{k}_{\pm}\cdot\vec{R})\begin{pmatrix}1\\ \pm\exp(-i\theta_0)\end{pmatrix}\\ &= \frac{1}{\sqrt{2}}\exp(i\vec{k}_{\pm}\cdot\vec{r}_k)\exp[ik_{\pm}r_{\vec{R},\vec{r}_k}\cos(\theta_0-\theta_{\vec{r}_k}^{\vec{R}})]\\ &\quad\times\begin{pmatrix}1\\ \pm\exp(-i\theta_0)\end{pmatrix} = \frac{1}{\sqrt{2}}\exp(i\vec{k}_{\pm}\cdot\vec{r}_k)\begin{pmatrix}1\\ \pm\exp(-i\theta_0)\end{pmatrix}\\ &\quad\times\left(\sum_{l=-\infty}^{\infty}J_l(k_{\pm}r_{\vec{R},\vec{r}_k})i^l\exp(il[\theta_{\vec{r}_k}^{\vec{R}}-\theta_0])\right),\end{aligned}\tag{15}$$

where $r_{\vec{R},\vec{r}_k}=|\vec{R}-\vec{r}_k|$ is the distance measured from the center of the scatterer and $\theta_{\vec{r}_k}^{\vec{R}}$ is the angle with respect to the $\hat{Y}$ axis of the vector $\vec{r}$, i.e.,

$$\exp(i\theta_{\vec{r}_k}^{\vec{R}}) = \frac{(\vec{R}-\vec{r}_k)\cdot\hat{Y}+i(\vec{R}-\vec{r}_k)\cdot\hat{X}}{r_{\vec{R},\vec{r}_k}}.\tag{16}$$

The wave function outside of the scatterer $|\vec{R}-\vec{r}_k|>a$ can therefore be written as

$$\Psi_{\text{I}}^{\pm}(\vec{R}) = \Phi_{\text{in}}^{\pm}(\vec{R})+\Psi_S^{\pm}(\vec{R}),\tag{17}$$

where the scattered wave function $\Psi_S^{\pm}(\vec{R})$ can be written as

$$\Psi_S^{\pm}(\vec{R}) = \sum_{l=-\infty}^{\infty} f_l^{\pm 1}\chi_{l,\uparrow}^{+}(\vec{R},E)+f_l^{\pm 2}\chi_{l,\downarrow}^{+}(\vec{R},E).\tag{18}$$

The wave function inside the cylindrical potential $\Psi_{\text{II}}^{\pm}(\vec{R})$ can be similarly written for $|\vec{R}-\vec{r}_k|\leqslant a$ as

$$\begin{aligned}\Psi_{\text{II}}^{\pm}(\vec{R}) &= \sum_{l=-\infty}^{\infty} d_l^{\pm 1}\frac{1}{2}[\chi_{l,\uparrow}^{+}(\vec{R},E-V_0)+\chi_{l,\uparrow}^{-}(\vec{R},E-V_0)]\\ &\quad+d_l^{\pm 2}\frac{1}{2}[\chi_{l,\downarrow}^{+}(\vec{R},E-V_0)+\chi_{l,\downarrow}^{-}(\vec{R},E-V_0)].\end{aligned}\tag{19}$$

Note that Eq. (19) contains both incoming and outgoing states [as given in Eq. (11)] in order to remove the Y_l terms in $\chi_{l,\uparrow(\downarrow)}^{\pm}$, which are singular at $\vec{R}=\vec{r}_k$.

From the continuity equations of the Schrodinger equations, $\Psi_{\text{I}}^{\pm}(\vec{R})$ and $\Psi_{\text{II}}^{\pm}(\vec{R})$ must satisfy the following conditions for all $\vec{R}$ such that $|\vec{R}-\vec{r}_k|=a$:

$$\Psi_{\text{I}}^{\pm}(|\vec{R}-\vec{r}_k|=a) = \Psi_{\text{II}}^{\pm}(|\vec{R}-\vec{r}_k|=a),\tag{20}$$

$$\begin{aligned}&\frac{\hbar^2}{2m^*}\left.\frac{\partial\Psi_{\text{I}}^{\pm}(\vec{R})}{\partial r}\right|_{|\vec{R}-\vec{r}_k|=a}+\left[\frac{\hbar^2}{2m^*a}\right.\\ &\quad\left.-i\alpha\begin{pmatrix}0 & \exp(i\theta_{\vec{r}_k}^{\vec{R}})\\ \exp(-i\theta_{\vec{r}_k}^{\vec{R}}) & 0\end{pmatrix}\right]\Psi_{\text{I}}^{\pm}(|\vec{R}-\vec{r}_k|=a)\\ &= \frac{\hbar^2}{2m^*}\left.\frac{\partial\Psi_{\text{II}}^{\pm}(\vec{R})}{\partial r}\right|_{|\vec{R}-\vec{r}_k|=a}+\left[\frac{\hbar^2}{2m^*a}\right.\\ &\quad\left.-i\alpha_{\text{II}}\begin{pmatrix}0 & \exp(i\theta_{\vec{r}_k}^{\vec{R}})\\ \exp(-i\theta_{\vec{r}_k}^{\vec{R}}) & 0\end{pmatrix}\right]\Psi_{\text{II}}^{\pm}(|\vec{R}-\vec{r}_k|=a).\end{aligned}\tag{21}$$

In the following discussion, $\alpha_{\text{II}}=\alpha$, i.e., the spin-orbit coupling strength is the same inside and outside the well.

The solutions for the various coefficients $d_l^{\pm}$ and $f_l^{\pm}$ are given in Appendix A for a cylindrical well/barrier. In the following, we are interested in studying the wave function away from the scatterer, so the relevant coefficients are $f_l^{\pm 1}$ and $f_l^{\pm 2}$, which can be written for convenience as

$$\begin{aligned}f_l^{\pm 1} &= 2i^l\exp(i\vec{k}_{\pm}\cdot\vec{r}_k)\exp(-il\theta_0)\frac{\tilde{f}_l^{\pm 1}}{\sqrt{k_1}},\\ f_l^{\pm 2} &= 2i^l\exp(i\vec{k}_{\pm}\cdot\vec{r}_k)\exp(-il\theta_0)\frac{\tilde{f}_l^{\pm 2}}{\sqrt{k_2}}.\end{aligned}\tag{22}$$

The coefficients $\tilde{f}_l^{\pm 1}$ and $\tilde{f}_l^{\pm 2}$ depend upon the energy and the form of the potential but do not depend upon the initial direction of the incident momentum vector θ_0 (different potentials will generate a different dependence of the coefficients upon θ_0, E, etc.). Thus the scattered wave function $\Psi_S^{\pm}(\vec{R})$ can be written as

$$\Psi_S^{\pm}(\vec{R}) = \sum_{l=-\infty}^{\infty} i^l\exp(il[\theta_{\vec{r}_k}^{\vec{R}}-\theta_0])(\tilde{T}_{k,l}\Phi_{\text{in}}^{\pm}(\vec{R}))_{\vec{R}=\vec{r}_k},\tag{23}$$

where

$$\tilde{T}_{k,l} = [\tilde{f}_l^{+1}\chi_{l,\uparrow}^{+}(\vec{R}-\vec{r}_k,E)\langle +(\theta_0)| + \tilde{f}_l^{-1}\chi_{l,\uparrow}^{+}(\vec{R}-\vec{r}_k,E)\langle -(\theta_0)|] + [\tilde{f}_l^{+2}\chi_{l,\downarrow}^{+}(\vec{R}-\vec{r}_k,E)\langle +(\theta_0)| + \tilde{f}_l^{-2}\chi_{l,\downarrow}^{+}(\vec{R}-\vec{r}_k,E)\langle -(\theta_0)|]$$
$$= \frac{1}{2}\begin{pmatrix} H_l(k_1 r_{\vec{R},\vec{r}_k})A_l^1 & \exp(i\theta_0)H_l(k_1 r_{\vec{R},\vec{r}_k})B_l^1 \\ -\exp(-i\theta_{\vec{r}_k}^{\vec{R}})iH_{l-1}(k_1 r_{\vec{R},\vec{r}_k})A_l^1 & -\exp[i(\theta_0-\theta_{\vec{r}_k}^{\vec{R}})]iH_{l-1}(k_1 r_{\vec{R},\vec{r}_k})B_l^1 \end{pmatrix}$$
$$+ \frac{1}{2}\begin{pmatrix} H_l(k_2 r_{\vec{R},\vec{r}_k})A_l^2 & \exp(i\theta_0)H_l(k_2 r_{\vec{R},\vec{r}_k})B_l^2 \\ \exp(-i\theta_{\vec{r}_k}^{\vec{R}})iH_{l-1}(k_2 r_{\vec{R},\vec{r}_k})A_l^2 & \exp[i(\theta_0-\theta_{\vec{r}_k}^{\vec{R}})]iH_{l-1}(k_2 r_{\vec{R},\vec{r}_k})B_l^2 \end{pmatrix}, \tag{24}$$

where

$$\tilde{A}_l^j = \tilde{f}_l^{+j} + \tilde{f}_l^{-j},$$
$$\tilde{B}_l^j = \tilde{f}_l^{+j} - \tilde{f}_l^{-j}, \tag{25}$$

where $H_l \equiv H_l^+$ in Eq. (24) (the + sign will be implicitly assumed for the Hankel function for the rest of this paper).

The operators $\tilde{T}_{k,l}$ in Eqs. (23) and (24) appear to generate the lth partial wave from the incident wave function Φ_{in} evaluated at the site of the scatterer. The only problem with this interpretation are the various factors of $\exp(il\theta_0)$ occurring in Eqs. (23) and (24). Since different incident waves will possess or be a superposition of different incident momentum directions (i.e., θ_0 in Fig. 1), an additional operator needs to be constructed which generates the various factors of $\exp(il\theta_0)$ from the incident wave with energy E. The operator $\hat{D}_l$ can be constructed such that for any given state of the form $|\Phi_{\text{in}}\rangle = c_1|k_1(\theta_0),+(\theta_0)\rangle + c_2|k_2(\theta_0),-(\theta_0)\rangle$,

$$\hat{D}_l\Phi_{\text{in}}(\vec{R}) = \exp(il\theta_0)\Phi_{\text{in}}(\vec{R}). \tag{26}$$

The operator $\hat{D}_l$ which satisfies the above equation is given by

$$\hat{D}_l = \begin{pmatrix} a_l\hat{P}_l & b_l\hat{P}_{l+1} \\ c_l\hat{P}_{l-1} & d_l\hat{P}_l \end{pmatrix}, \tag{27}$$

where

$$\hat{P}_l = \left(\frac{l}{|l|}\frac{\partial}{\partial(\vec{R}\cdot\hat{X})} - i\frac{\partial}{\partial(\vec{R}\cdot\hat{Y})}\right)^{|l|} \tag{28}$$

with $\hat{P}_0 = 1$. The construction and full expression for $\hat{D}_l$ is given in the Appendix B.

The operator which generates the scattered wave from the wave incident upon scatterer k, $\hat{T}_k$, can finally be written as

$$\hat{T}_k = \sum_{l=-\infty}^{\infty} i^l \exp(-il\theta_{\vec{r}_k}^{\vec{R}})\hat{G}_l^k\hat{P}_l, \tag{29}$$

where

$$\hat{G}_l^k = \frac{1}{2}\begin{pmatrix} H_l(k_1 r_{\vec{R},\vec{r}_k}) & -i\exp(i\theta_{\vec{r}_k}^{\vec{R}})H_{l-1}(k_1 r_{\vec{R},\vec{r}_k}) \\ i\exp(-i\theta_{\vec{r}_k}^{\vec{R}})H_{l+1}(k_1 r_{\vec{R},\vec{r}_k}) & H_l(k_1 r_{\vec{R},\vec{r}_k}) \end{pmatrix}\begin{pmatrix} t_{k,l}^{11} & 0 \\ 0 & t_{k,l}^{12} \end{pmatrix}$$
$$+ \frac{1}{2}\begin{pmatrix} H_l(k_2 r_{\vec{R},\vec{r}_k}) & i\exp(i\theta_{\vec{r}_k}^{\vec{R}})H_{l-1}(k_2 r_{\vec{R},\vec{r}_k}) \\ -i\exp(-i\theta_{\vec{r}_k}^{\vec{R}})H_{l+1}(k_2 r_{\vec{R},\vec{r}_k}) & H_l(k_2 r_{\vec{R},\vec{r}_k}) \end{pmatrix}\begin{pmatrix} t_{k,l}^{21} & 0 \\ 0 & t_{k,l}^{22} \end{pmatrix}, \tag{30}$$

where $t_{k,l}^{11} = A_{-l}^{k,1}a_l + B_{-l}^{k,1}c_{1+l}$, $t_{k,l}^{l2} = A_{1-l}^{k,1}b_{l-1} + B_{1-l}^{k,1}d_l$, $t_{k,l}^{21} = A_{-l}^{k,2}a_l + B_{-l}^{k,2}c_{1+l}$, and $t_{k,l}^{22} = -A_{1-l}^{k,2}b_{l-1} - B_{1-l}^{k,2}d_l$. From the values for the various $f_l^{k,\pm1}$ and $f_l^{k,\pm2}$ calculated in Appendix A for a cylindrically symmetric barrier/well, it can be shown that $t_{k,l}^{11} = t_{k,-l}^{12}$ and $t_{k,l}^{21} = t_{k,-l}^{22}$. Note that the form of $\hat{T}_k$ is the same for all cylindrically symmetric scatterers; the values of the scattering amplitudes $\tilde{f}_l^{\pm j}$ depend upon the actual potential used for the cylindrically symmetric scatterer.

III. MULTIPLE SCATTERING THEORY

For N isolated scatterers, the overall wave function at $\vec{R}$ can be written as

$$\Psi(\vec{R}) = \Phi_{\text{in}}(\vec{R}) + \sum_{k=1}^{N}[\hat{T}_k\Psi(\vec{R})]_{\vec{R}=\vec{r}_k}. \tag{31}$$

Equation (31) indicates that if the value of $\Psi(\vec{R})$ and its derivatives [due to the $\hat{P}_l$ dependence of $\hat{T}_k$ in Eq. (29)] at each scatterer is known, the entire wave function $\Psi(\vec{R})$ is completely determined. In principle, the values of $\Psi(\vec{R})$ and its derivatives

at each scatterer can be found using Eq. (31). In practice, it is only practical to calculate the first few derivatives of $\Psi(\vec{R})$ at each scatterer. When the size of the scatterer (or in general, the scattering length) is much smaller than the wavelengths, i.e., $k_1 a \ll 1$ and $k_2 a \ll 1$, the only significant contribution to $\hat{T}_k$ comes from the $l=0$ term in Eq. (29). This is analogous to the heavily studied "s-wave" scattering models, and in the following discussion, only the $l=0$ term in Eq. (29) will be considered.

IV. LOW-ENERGY SCATTERING LIMIT

In the limit $k_{1(2)} a \ll 1$, Eq. (31) can be approximated as

$$\Psi(\vec{R}) = \Phi_{\text{in}}(\vec{R}) + \sum_{k=1}^{N} G_0^k(\vec{R})\Psi(\vec{r}_k), \tag{32}$$

where G_0^k can be written as

$$G_0^k(\vec{R}) = \frac{1}{2}\begin{pmatrix} H_0(k_1 r_{\vec{R},\vec{r}_k}) & i\exp(i\theta_{\vec{r}_k}^{\vec{R}}) H_1(k_1 r_{\vec{R},\vec{r}_k}) \\ i\exp(-i\theta_{\vec{r}_k}^{\vec{R}}) H_1(k_1 r_{\vec{R},\vec{r}_k}) & H_0(k_1 r_{\vec{R},\vec{r}_k}) \end{pmatrix} t_{k,0}^1 + \frac{1}{2}\begin{pmatrix} H_0(k_2 r_{\vec{R},\vec{r}_k}) & -i\exp(i\theta_{\vec{r}_k}^{\vec{R}}) H_1(k_2 r_{\vec{R},\vec{r}_k}) \\ -i\exp(-i\theta_{\vec{r}_k}^{\vec{R}}) H_1(k_2 r_{\vec{R},\vec{r}_k}) & H_0(k_2 r_{\vec{R},\vec{r}_k}) \end{pmatrix} t_{k,0}^2. \tag{33}$$

It should be noted that Eqs. (32) and (33) are similar to the Lippmann-Schwinger equation for a potential $V_\delta(\vec{r})$ comprised of N delta functions $V_\delta(\vec{r}) = \Sigma_k V_k \delta(\vec{r} - \vec{r}_k)$, which has been used before in previous studies of the spin dynamics in the presence of spin-orbit coupling.[8,10,18] From the Lippmann-Schwinger equation, the wave function in the presence of $V_\delta(\vec{r})$ is given by

$$\begin{aligned}\Psi(\vec{R}) &= \Phi_{\text{in}}(\vec{R}) + \int \hat{G}_+(\vec{R},\vec{r},E) V_\delta(\vec{r}) \Psi(\vec{r}) d^3 r \\ &= \Phi_{\text{in}}(\vec{R}) + \sum_{k=1}^{N} V_k \hat{G}_+(\vec{R},\vec{r}_k,E)\Psi(\vec{r}_k),\end{aligned} \tag{34}$$

where $\hat{G}_+(\vec{R},\vec{r}_k,E)$ is the Green's function in the presence of Rashba spin-orbit coupling, which is given by Eq. (C13) in Appendix C and is similar in form to $G_0^k(\vec{R})$. The form of $G_0^k(\vec{R})$ would be identical to $\hat{G}_+(\vec{R},\vec{r}_k)$ if

$$\frac{t_{k,0}^1}{t_{k,0}^2} = \frac{k_1}{k_2}. \tag{35}$$

In general, Eq. (35) is not satisfied, although for $\bar{k} a \ll 1$ Eq. (35) is approximately correct. The difference $\hat{G}_+(\vec{R},\vec{r}_k,E)$, and $\hat{G}_0^k(\vec{R})$ can be understood as follows: $\hat{G}_+(\vec{R},\vec{r}_k,E)$ propagates the scattered wave function from the δ-function potential, whereas $\hat{G}_0^k(\vec{R})$ propagates the scattered wave function from the finite-sized potential $V_k(\vec{r})$ [Eq. (14)], which, in the δ function limit ($a \to 0$, $V_0 \to \pm\infty$, $\pi V_0 a^2 = \pm V_k$), does not scatter (i.e., the scattering coefficients $t_{k,0}^1$ and $t_{k,0}^2$ vanish).

Far away from the scatterers ($k_{1(2)} r_{\vec{R},\vec{r}_k} \gg 1$), Eq. (33) can be written as

$$\begin{aligned}G_0^k(\vec{R}) = &\sqrt{\frac{2}{\pi r_{\vec{R},\vec{r}_k}}} \exp\left(i\left[\bar{k} r_{\vec{R},\vec{r}_k} - \frac{\pi}{4} + \phi_k\right]\right) \\ &\times \left[\bar{t}_k - i\overline{\delta t}_k \hat{U}\left(\frac{\pi}{2}, \theta_{\vec{r}_k}^{\vec{R}}\right)\right] \hat{U}(k_\alpha r_{\vec{R},\vec{r}_k} + \delta\phi_k, \theta_{\vec{r}_k}^{\vec{R}}),\end{aligned} \tag{36}$$

where

$$\begin{aligned}\bar{k} &= \frac{k_1 + k_2}{2} = \sqrt{\left(\frac{m^* \alpha}{\hbar^2}\right)^2 + \frac{2m^*}{\hbar^2} E}, \\ k_\alpha &= \frac{k_1 - k_2}{2} = \frac{\alpha m^*}{\hbar^2}, \\ \bar{t}_k &= \frac{|\hat{t}_{k,0}^1|\sqrt{k_2} + |\hat{t}_{k,0}^2|\sqrt{k_1}}{2\sqrt{k_1 k_2}}, \\ \overline{\delta t}_k &= \frac{|\hat{t}_{k,0}^1|\sqrt{k_2} - |\hat{t}_{k,0}^2|\sqrt{k_1}}{2\sqrt{k_1 k_2}}, \\ \exp(i\delta\phi_k) &= \sqrt{\frac{\hat{t}_{k,0}^1 (\hat{t}_{k,0}^2)^*}{|\hat{t}_{k,0}^1 \hat{t}_{k,0}^2|}}, \\ \exp(i\phi_k) &= \sqrt{\frac{\hat{t}_{k,0}^1 \hat{t}_{k,0}^2}{|\hat{t}_{k,0}^1 \hat{t}_{k,0}^2|}}\end{aligned} \tag{37}$$

and $\hat{U}(\theta,\phi)$ is a rotation operator given by

$$\hat{U}(\theta,\phi) = \exp\left(i\frac{\phi}{2}\hat{\sigma}_Z\right)\exp(i\theta\hat{\sigma}_X)\exp\left(-i\frac{\phi}{2}\hat{\sigma}_Z\right). \tag{38}$$

Equation (33) contains a dynamical factor which depends upon the distance from scatterer k multiplied by a sum of two

rotation operators. In the presence of spin-orbit coupling, the low-energy limit scattered wave functions possess an "*s*-wave" character and also a "*p*-wave" character due to the $\theta^{\vec{R}}_{\vec{r}_k}$ dependence in Eq. (33), which vanishes in the limit as $\alpha \to 0$.

In the calculations to be performed, $\delta t_k/\bar{t}_k \approx 0.05$ and $\delta\phi_k \ll 1$. In this case, Eq. (33) can be approximately written as [for $k_{1(2)}|\vec{R}-\vec{r}_k| \gg 1$]:

$$G_0^k(\vec{R}) = \bar{t}_k \sqrt{\frac{2}{\pi r_{\vec{R},\vec{r}_k}}} \exp\left(i\left[\bar{k} r_{\vec{R},\vec{r}_k} - \frac{\pi}{4} + \phi_k \right] \right) \hat{U}(k_\alpha r_{\vec{R},\vec{r}_k}, \theta^{\vec{R}}_{\vec{r}_k}) \tag{39}$$

which now contains a dynamical, distance-dependent factor times a single rotation operator $\hat{U}(k_\alpha r_{\vec{R},\vec{r}_k}, \theta^{\vec{R}}_{\vec{r}_k})$, which corresponds to a rotation by an angle $k_\alpha r_{\vec{R},\vec{r}_k}$ about the spin-orbit field for propagation along the direction $(\vec{R}-\vec{r}_k)/|\vec{R}-\vec{r}_k|$. In this limit, the total wave function in the presence of N scatterers is given by

$$\Psi(\vec{R}) = \Phi(\vec{R}) + \sum_j \bar{t}_j \sqrt{\frac{2}{\pi r_{\vec{R},\vec{r}_j}}} \exp\left(i\left[\bar{k} r_{\vec{R},\vec{r}_j} - \frac{\pi}{4} + \phi_j \right] \right) \times \hat{U}(k_\alpha r_{\vec{R},\vec{r}_j}, \theta^{\vec{R}}_{\vec{r}_j}) \Psi(\vec{r}_j). \tag{40}$$

From Eq. (40), knowing the value of the wave function at each scatterer k, $\Psi(\vec{r}_k)$, completely determines the total wave function $\Psi(\vec{R})$. The various values of $\Psi(\vec{r}_k)$ can be found by setting $\vec{R}=\vec{r}_k$ in Eq. (32) for each scatterer k. This provides a system of $2N$ linear equations to solve for the various $\Psi(\vec{r}_k)$. The resulting system of equations can be expressed in matrix form as

$$\hat{M}\hat{\Psi} = \hat{\phi}, \tag{41}$$

where $\hat{\Psi}$ and $\hat{\phi}$ are $2N$ by 1 matrices where $\hat{\Psi}(2k-1) = \Psi^{\uparrow}(\vec{r}_k)$, $\hat{\Psi}(2k) = \Psi^{\downarrow}(\vec{r}_k)$, $\hat{\phi}(2k-1) = \phi^{\uparrow}(\vec{r}_k)$, $\hat{\phi}(2k) = \phi^{\downarrow}(\vec{r}_k)$, and $\hat{M}$ is a $2N$ by $2N$ matrix where $\hat{M}(m,m)=1$ for $m=1$ to $m=2N$, and for $k,j \in [1,N]$ and $k \neq j$,

$$\hat{M}(2k-1,2j-1) = -[G_0^j(\vec{r}_k)]_{1,1},$$

$$\hat{M}(2k,2j) = -[G_0^j(\vec{r}_k)]_{2,2},$$

$$\hat{M}(2k-1,2j) = -[G_0^j(\vec{r}_k)]_{1,2},$$

$$\hat{M}(2k,2j-1) = -[G_0^j(\vec{r}_k)]_{2,1}, \tag{42}$$

where $G_0^j(\vec{r}_k)$ is given in Eq. (33). Once $\hat{M}$ is specified, $\hat{\Psi}$ can be found by inverting $\hat{M}$ as follows:

$$\hat{\Psi} = \hat{M}^{-1}\hat{\phi}. \tag{43}$$

V. APPLICATIONS TO FLUX MEASUREMENTS IN TWO-DIMENSIONAL ELECTRON GASES IN THE PRESENCE OF RASHBA SPIN-ORBIT COUPLING

Recent experiments[13,19,20] have imaged electron flow through a quantum point contact (QPC) in a 2DEG by monitoring the changes in conductance through the QPC as a moveable SPM tip is scanned above the surface of a heterostructure. The SPM tip generates a Lorentzian-shaped potential in the 2DEG with its height determined by the voltage of the SPM tip and its width given by the distance from the tip to the 2DEG.[21] This tip-induced potential can backscatter electrons in the 2DEG. As the SPM tip is scanned above the surface of the heterostructure, the backscattered current into the QPC is monitored, and the change in conductance is mapped out as a function of SPM tip position. Placing the tip over regions of large electron flow results in a larger change in conductance (since more electrons are backscattered in this case) than placing the tip over regions of low electron flow (where fewer electrons are backscattered). In this manner, a map of the electron flow is generated. Numerical studies[13,20,22,23] have demonstrated that the resulting conductance images mirrors the actual electron flow in the 2DEG. However, interference effects induced by the SPM tip itself are also observed on top of the electrons flow pattern. Interference between the single scattering trajectory from the SPM tip with the single scattering trajectories from random impurities within the sample generates interference fringes spaced at half the Fermi wavelength atop the conductance maps;[13,19,20,22] these fringes are not in the actual electron flow. Recently, additional interference effects for electrons emitted from a single QPC were also reported for an SPM tip in the presence of a fixed reflector gate.[24] In this experiment, interference fringes result not only from the interference between the single scattering trajectories of the reflector gate and the SPM tip but also from the interference of the double scattering trajectories involving the reflector gate and the single scattering trajectory from the SPM tip. The observed interference fringes due to these multiple-scattering trajectories can complicate backing out the actual electron flow from the conductance map.[25–27]

The samples used in the above experimental studies were GaAs/AlGaAs heterostructures, which have very low spin-orbit coupling[28] ($\alpha = 3 \times 10^{-13}$ eV m), and the experimental results were well described by quantum simulations and calculations in the absence of spin-orbit coupling.[13,14,19,22,24,29] However, other samples can possess considerably larger spin-orbit coupling,[30] such as InAs, which can have $\alpha = 4 \times 10^{-11}$ eV m. The question therefore arises as to what effects or signatures of spin-orbit coupling exist in electron flow imaging experiments using a moveable SPM tip.

Figure 2 shows the setup under consideration. A point source is used to inject electrons into the 2DEG (analogous to a QPC). The injected electrons are backscattered by random impurities present in the sample and by the potential generated by the SPM tip placed above the surface of the 2DEG. The backscattered current into the detection QPC is then measured as a function of the SPM tip position $\vec{R}_t$. In the setup shown in Fig. 2, the possibility that the detection

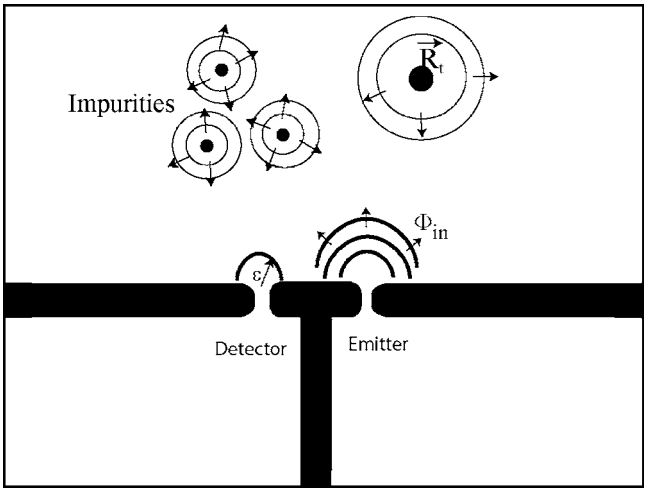

FIG. 2. Electrons injected by the emitter QPC (represented by Φ_{in}) are backscattered due to random impurities in the 2DEG along with a moveable "scatterer" generated by an SPM above the 2DEG surface. Measurements of the backscattered flux into the detector QPC as a function of the SPM tip position $\vec{R}_t$ can be used to image the electron flow from the emitter.

QPC can be separate from the emitter QPC is allowed. Such experimental geometries have been used in magnetic focussing experiments in the past.[31]

The injected electrons from the emitter are taken to be an unpolarized beam comprised of an equal mixture of the cylindrical wavelike states $\Phi_1(\vec{R})$ and $\Phi_2(\vec{R})$, which are given by

$$\Phi_1(\vec{R}) = \exp\left(i\frac{\pi}{4}\right)[\chi_{0,\uparrow}(\vec{R}) + \chi_{0,\downarrow}(\vec{R})],$$

$$\Phi_2(\vec{R}) = i\exp\left(i\frac{\pi}{4}\right)[\chi_{1,\uparrow}(\vec{R}) - \chi_{1,\downarrow}(\vec{R})]. \tag{44}$$

Each state represents current of $\hbar\bar{k}/m^*$ being injected into the emitter, as shown in Fig. 2. Far away from the source, the states can be approximated as

$$\Phi_1(\vec{R}) = \frac{1}{\sqrt{\pi|\vec{R}|}}\exp(i\bar{k}|\vec{R}|)\hat{U}(k_\alpha|\vec{R}|,\theta_e)\begin{pmatrix}1\\0\end{pmatrix}, \tag{45}$$

$$\Phi_2(\vec{R}) = \frac{1}{\sqrt{\pi|\vec{R}|}}\exp(i\bar{k}|\vec{R}|)\hat{U}(k_\alpha|\vec{R}|,\theta_e)\begin{pmatrix}0\\1\end{pmatrix}, \tag{46}$$

where θ_e is the given with respect to the emitter. Note that when $\alpha\to 0$, the states Φ_1 and Φ_2 correspond to a spin up and spin down electron being injected from the point source.

The net current injected into the detector is given by the following formula:

$$\mu = \epsilon\int_{-\pi/2}^{\pi/2} d\theta[J_X(\vec{\epsilon})\sin(\theta) + J_Y(\vec{\epsilon})\cos(\theta)], \tag{47}$$

where

$$J_X(\vec{\epsilon}) = \frac{\hbar}{m^*}\,\mathrm{Im}[\Psi^\dagger(\vec{R})\nabla_X\Psi(\vec{R})]_{\vec{R}=\vec{\epsilon}} + \frac{\alpha}{\hbar}\Psi^\dagger(\vec{\epsilon})\hat{\sigma}_Y\Psi(\vec{\epsilon}),$$

$$J_Y(\vec{\epsilon}) = \frac{\hbar}{m^*}\,\mathrm{Im}[\Psi^\dagger(\vec{R})\nabla_Y\Psi(\vec{R})]_{\vec{R}=\vec{\epsilon}} - \frac{\alpha}{\hbar}\Psi^\dagger(\vec{\epsilon})\hat{\sigma}_X\Psi(\vec{\epsilon}), \tag{48}$$

and $\vec{\epsilon}=\epsilon[\cos(\theta)\hat{Y}+\sin(\theta)\hat{X}]$. In the actual experiment/simulation, the current injected into the detector is measured as a function of tip position several microns away from the detector. As will be discussed later, the interference between the incident waves and the scattered waves can be neglected in Eq. (47) due to thermal averaging, so only the scattered wave function Ψ_S needs to be considered. Phase-coherent transport is assumed in the application of Eq. (47). Additionally, since the width of the detector is taken to be negligible, only the current operator of Ψ_S evaluated at the detector needs to taken into account in Eq. (47). The injected current into the detector becomes

$$\mu = 2\epsilon\left(\frac{\hbar}{m^*}\,\mathrm{Im}[\Psi_S^\dagger(\vec{R}_d)\nabla_Y\Psi_S(\vec{R}_d)] - \frac{\alpha}{\hbar}\Psi_S^\dagger(\vec{R}_d)\hat{\sigma}_X\Psi_S(\vec{R}_d)\right). \tag{49}$$

Using the form of the wave function in Eq. (40) evaluated at the site of the detector, the injected current can then be written as a function of tip position and energy as

$$\mu(\vec{R}_t,E) = \frac{4\epsilon}{\pi}\sum_k \frac{\bar{t}_k^2}{r_{k,d}}\cos(\theta_k^d)\frac{\hbar\bar{k}}{m^*}\Psi^\dagger(\vec{r}_k)\Psi(\vec{r}_k) - \frac{\bar{t}_k^2}{r_{k,d}}\frac{\alpha}{\hbar}\Psi^\dagger(\vec{r}_k)\hat{U}^\dagger(k_\alpha r_{k,d},\theta_k^d)\left[\frac{\sin(2\theta_k^d)}{2}\hat{\sigma}_Y + \sin^2(\theta_k^d)\hat{\sigma}_X\right]\hat{U}(k_\alpha r_{k,d},\theta_k^d)\Psi(\vec{r}_k)$$
$$+ \frac{4\epsilon}{\pi}\frac{\hbar\bar{k}}{m^*}\sum_{j<k}\bar{t}_k\bar{t}_j\left(\frac{\cos(\theta_k^d)+\cos(\theta_j^d)}{2\sqrt{r_{k,d}r_{j,d}}}\right)(\Psi^\dagger(\vec{r}_k)\hat{U}^\dagger(k_\alpha r_{k,d},\theta_k^d)\hat{U}(k_\alpha r_{j,d},\theta_j^d)\Psi(\vec{r}_j)$$
$$\times\exp\{i[\bar{k}(r_{j,d}-r_{k,d})+\phi_j-\phi_k]\}+\mathrm{H.c.}) + \frac{4\epsilon}{\pi}\frac{\alpha}{\hbar}\sum_{j<k}\frac{\bar{t}_k\bar{t}_j}{\sqrt{r_{j,d}r_{k,d}}}\left(\frac{[\cos(\theta_j^d)]^2+[\cos(\theta_k^d)]^2}{2}-1\right)$$
$$\times\{\Psi^\dagger(\vec{r}_k)\hat{U}^\dagger(k_\alpha r_{k,d},\theta_k^d)\hat{\sigma}_X\hat{U}(k_\alpha r_{j,d},\theta_j^d)\Psi(\vec{r}_j)\exp[i\bar{k}(r_{j,d}-r_{k,d})+\phi_j-\phi_k]+\mathrm{H.c.}\}$$

$$-\frac{4\epsilon}{\pi}\frac{\alpha}{\hbar}\sum_{j<k}\frac{\bar{t}_k\bar{t}_j}{\sqrt{r_{j,d}r_{k,d}}}\frac{\sin(\theta_j^d)\cos(\theta_j^d)+\sin(\theta_k^d)\cos(\theta_k^d)}{2}$$

$$\times\{\Psi^\dagger(\vec{r}_k)\hat{U}^\dagger(k_\alpha r_{k,d},\theta_k^d)\hat{\sigma}_Y\hat{U}(k_\alpha r_{j,d},\theta_j^d)\Psi(\vec{r}_j)\exp[i\bar{k}(r_{j,d}-r_{k,d})+\phi_j-\phi_k]+\text{H.c.}\}, \tag{50}$$

where the energy dependence of $\mu(\vec{R}_t,E)$ comes in through the energy dependence of both $\bar{k}$ and $\bar{t}_k$. Since all experiments are done at nonzero temperatures, thermal averaging of Eq. (50) becomes necessary. Assuming the injected current is a result of a small potential drop δV over the emitter QPC and that the electrons on both sides of the emitter QPC can be described as being free 2DEG, the energy weighting function is simply related to the Fermi-Dirac distribution function $f(E)$ and is given by

$$-f'(E)dE=\frac{dE}{k_BT}\frac{\exp\left(\frac{E-E_F}{k_BT}\right)}{\left[1+\exp\left(\frac{E-E_F}{k_BT}\right)\right]^2}, \tag{51}$$

where E_F is the Fermi energy. All quantities calculated will be thermally averaged using Eq. (51). The thermally averaged injected current is then given by

$$\overline{\mu(\vec{R}_t)}=-\int_0^\infty\mu(\vec{R}_t,E)f'(E)dE. \tag{52}$$

Since $\mu(\vec{R}_t)$ contains interference terms that go as $\bar{k}\exp(i\bar{k}r)$ (where r is some length related to the various distances in the system), the following integral[32] will be useful in evaluating Eq. (52):

$$-\int_0^\infty\bar{k}f'(E)\exp(i\bar{k}r)dE=-2i\lambda_T\exp(i\bar{k}_Fr)\sinh^{-1}(\lambda_Tr)[1-\lambda_Tr\coth(\lambda_Tr)]+\frac{\lambda_T}{\bar{k}_F}\exp(i\bar{k}_Fr)\sinh^{-1}(\lambda_Tr)[\bar{k}_F^2r-2\lambda_T\coth(\lambda_Tr)]$$

$$-\frac{\lambda_T}{\bar{k}_F}\exp(i\bar{k}_Fr)\sinh^{-1}(\lambda_Tr)\lambda_T^2r[\coth^2(\lambda_Tr)+\sinh^{-2}(\lambda_Tr)]\equiv\exp(i\bar{k}_Fr)\sinh^{-1}(\lambda_Tr)g(r,T,E_F), \tag{53}$$

where $\lambda_T=\bar{k}_F\pi k_BT(2E_F)^{-1}$. For large r, interference terms in $\mu(\vec{R}_t)$ decay as $r\exp(-\lambda_Tr)$. For $T=3$ K, $E_F=16$ meV, $m^*=0.022m_0$ (where m_0 is the free electron mass), $\lambda_T=2.35\ \mu\text{m}^{-1}$, which allows one to neglect the interference between the incoming wave and scattered wave when calculating $\mu(\vec{R}_t)$ many microns away from the QPC.

A. The single-scattering limit

Before considering the case of multiple scattering (which can only be analytically solved for simple cases), it is useful to consider the single-scattering case for an unpolarized beam (i.e., averaged over the incident waves Φ_1 [Eq. (44)] and Φ_2 [Eq. (44)]). In this case, the value of the wave function at scatterer k is given by

$$\Psi_1(\vec{r}_k)=\frac{1}{\sqrt{\pi r_{e,k}}}\exp(i\bar{k}r_{e,k})\hat{U}(k_\alpha r_{e,k},\theta_e^k)\begin{pmatrix}1\\0\end{pmatrix} \tag{54}$$

for incident wave Φ_1 [Eq. (45)] and

$$\Psi_2(\vec{r}_k)=\frac{1}{\sqrt{\pi r_{e,k}}}\exp(i\bar{k}r_{e,k})\hat{U}(k_\alpha r_{e,k},\theta_e^k)\begin{pmatrix}0\\1\end{pmatrix} \tag{55}$$

for incident wave Φ_2 [Eq. (46)].

First consider the case when the detector and the emitter are one and the same. The spin averaged (i.e., averaged over incident waves Φ_1 and Φ_2) and thermally averaged change in flux as a function of tip position $\Delta\mu(\vec{R}_t,E)=\mu(\vec{R}_t,E)-\mu(\vec{R}_t=\infty,E)$ is given by

$$\overline{\Delta\mu(\vec{R}_t)} \approx \frac{2\epsilon}{\pi^2}\frac{\hbar\bar{k}_F}{m^*}\left[1+\frac{\pi^2}{12}\left(\frac{k_BT}{E_F}\right)^2\right]\bar{t}_t^2\frac{\cos(\theta_t^d)}{(r_{\mathrm{tip},d})^2}+\frac{2\epsilon}{\pi^2}\frac{\hbar}{m^*}\sum_k\frac{\cos(\theta_k^d)+\cos(\theta_t^d)}{r_{\mathrm{tip},d}r_{k,d}}\bar{t}_k\bar{t}_t\exp[i2\bar{k}_F2(r_{\mathrm{tip},d}-r_{k,d})+\phi_t-\phi_k]$$
$$\times\sinh^{-1}[2\lambda_T(r_{\mathrm{tip},d}-r_{k,d})]g[2(r_{\mathrm{tip},d}-r_{k,d}),T,E_F]+\mathrm{H.c.}$$
$$=\frac{2\epsilon}{\pi^2}\frac{\hbar\bar{k}_F}{m^*}\left[1+\frac{\pi^2}{12}\left(\frac{k_BT}{E_F}\right)^2\right]\bar{t}_t^2\frac{\cos(\theta_t^d)}{(r_{\mathrm{tip},d})^2}+F(\vec{R}_t)\exp(i2\bar{k}_Fr_{\mathrm{tip},d})+\mathrm{H.c.}, \tag{56}$$

where $F(\vec{R}_t)$ is some nonoscillatory function which depends on the particular configuration of scatterers, along with a some angular dependence of the tip and a exponential damping factor depending upon the tip position from the scatterers. Spin-orbit effects are not seen in Eq. (56) due to the fact that for electrons moving along effective one-dimensional trajectories, the amount of spin rotation induced is simply proportional to the net distance the electrons have traversed. Since an electron which is directly scattered back to the detector has effectively traveled no net distance, the net spin rotation is zero. Another way to see this is that $\hat{U}(k_\alpha r_{k,d},\theta_d^k)\hat{U}(k_\alpha r_{e,k},\theta_e^k)=\hat{1}$ when the emitter and detector are one and the same, since $r_{k,d}=r_{e,k}$ and $\theta_k^d=\theta_e^k+\pi$. As shown at the end of Appendix C, the above conclusions also hold if the approximation to $\hat{G}_0^k(\vec{R})$ in Eq. (39) is not made.

Consider the case explicitly illustrated in Fig. 2 where the detector and the emitter are two distinct entities. In this case, an electron does not traverse the same path back to the detector, and the effects of spin-orbit coupling do not average away in the flux calculation. Performing the thermal averaging and spin averaging [using Eqs. (45) and (46)], $\Delta\mu(\vec{R}_t)$ can be written as

$$\overline{\Delta\mu(\vec{R}_t)}=\frac{2\epsilon}{\pi^2}\frac{\hbar\bar{k}_F}{m^*}\left[1+\frac{\pi^2}{12}\left(\frac{k_BT}{E_F}\right)^2\right]\bar{t}_t^2\frac{\cos(\theta_t^d)}{r_{e,\mathrm{tip}}r_{\mathrm{tip},d}}+\exp(i\bar{k}_Fr_S)$$
$$\times[G_1(\vec{R}_t)\exp(ik_\alpha r_S)+G_2(\vec{R}_t)\exp(-ik_\alpha r_S)]$$
$$+\exp(i\bar{k}_Fr_S)[G_3(\vec{R}_t)\exp(ik_\alpha r_D)$$
$$+G_4(\vec{R}_t)\exp(-ik_\alpha r_D)]+\mathrm{H.c.}, \tag{57}$$

where $r_S=r_{e,\mathrm{tip}}+r_{\mathrm{tip},d}$ and $r_D=r_{\mathrm{tip},d}-r_{e,\mathrm{tip}}$, and where $G_1(\vec{R}_t)$, $G_2(\vec{R}_t)$, $G_3(\vec{R}_t)$, and $G_4(\vec{R}_t)$ are nonoscillatory functions of tip position which depend upon the particular configuration of scatterers. From Eq. (57), the expected elliptical fringes spaced at $\bar{k}_Fr_S=2n\pi$ with the detector and the emitter acting as the foci of the ellipse are present; however, the amplitude of these oscillations are now modulated by the Rashba spin-orbit coupling. Since the electron trajectories from the emitter to the detector QPC are now two dimensional, the electron's spin will undergo a trajectory-dependent spin rotation for each pathway between the emitter and the detector QPC. The interference between different pathways will thus have an additional, spin-dependent modulation. Such an amplitude modulation is similar to the D'yakonov-Perel' model of spin dephasing in the presence of spin-orbit coupling.[3,33] The first two oscillatory terms in Eq. (57) $G_1(\vec{R}_t)$ and $G_2(\vec{R}_t)$ lead to elliptical amplitude modulations of the regular fringes spaced at $k_\alpha r_S=2n\pi$, while the G_3 and G_4 terms in Eq. (57) lead to a hyperbolic amplitude modulation spaced at $k_\alpha r_D=2n\pi$, with the foci of the hyperbola again being the detector and the emitter. Interference between the terms G_1 and G_3 and between the terms G_2 and G_4 lead to fringes at $k_\alpha r_{e,\mathrm{tip}}=2n\pi$ for $r_{\mathrm{tip},d}=$const. Likewise, interference between the terms G_1 and G_4 and between the terms G_2 and G_3 lead to fringes at $k_\alpha r_{\mathrm{tip},d}=2n\pi$ for $r_{e,\mathrm{tip}}=$const. The presence of all four types of fringe patterns leads to a checkered pattern in $\Delta\mu(\vec{R}_t)$. This can be seen in the calculation of $\Delta\mu(\vec{R}_t)$ in Eq. (57) which is shown in Fig. 3(a). In this simulation, the emitter was placed at $\vec{r}_e=1.5\ \mu\mathrm{m}\ \hat{X}$ and the detector was placed 3 μm away at $\vec{r}_d=-1.5\ \mu\mathrm{m}\ \hat{X}$. In addition, the thermal average of $\Delta\mu(\vec{R}_t)$ was evaluated by numerically integrating Eq. (52) over the interval $E_F\pm6k_BT$, and the following parameters were used (similar to the parameters found for InAs[30]): $m^*=0.022m_0$ (where m_0 is the free electron mass), $E_F=16$ meV, $T=3$ K, and $\alpha=4\times10^{-11}$ eV m which gives a spin rotation length [i.e., the length required to rotate the spin by 180° of $l_\pi=\pi\hbar^2/(2m^*\alpha)$] of 134 nm. (For comparison, spin rotation lengths of $l_\pi\approx1.8$ μm were found for heterostructures of GaAs/AlGaAs in a past study.[28]) Scatterers were randomly placed in the region $[Y,X]=(0\ \mu\mathrm{m},6\ \mu\mathrm{m})\times(-6\ \mu\mathrm{m},6\ \mu\mathrm{m})$ with a scatterer density of 20 scatterers per $\mu\mathrm{m}^2$. All scatterers were modeled as cylindrical wells or barriers, with the well depths randomly chosen between ±.04 eV. The coupling constants, $\bar{t}_k$, were evaluated using Eq. (37) and the results in Appendix A. The radius of the barriers/wells were all taken to be $a=3$ nm, which gave $\bar{k}_Fa\approx0.3$ so that a model of s-wave scatterers could be used. The tip was modeled as a hard disc (i.e., infinite barrier) with the radius of the tip chosen to be $a=3$ nm. Although the width of the actual depletion area induced by the tip in the 2DEG is probably on the order of 100 nm, the above radius was chosen to be consistent with the s-wave model used in the calculations (further studies incorporating higher partial wave scattering in the presence of Rashba coupling are currently being carried out and will be addressed at a later time). Figure 3(a) is a typical result from the calculations performed on numerous scatterer configurations. In addition to the kinematical elliptical fringes spaced at $\bar{k}_Fr_S$

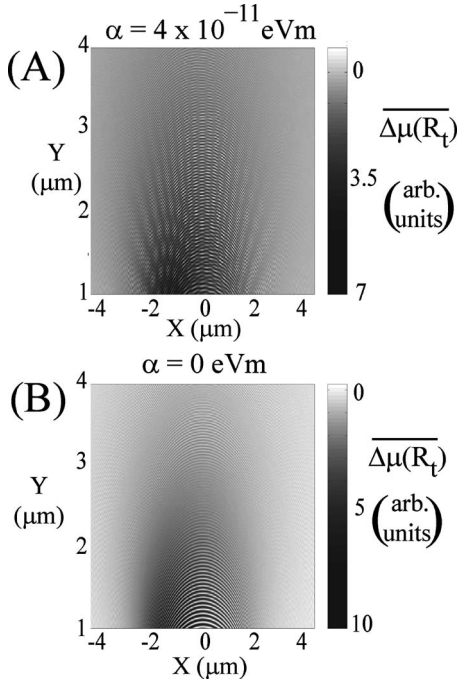

FIG. 3. Simulation of $\overline{\Delta\mu(\vec{R}_t)}$ [Eq. (57)] for an unpolarized beam of electrons injected from an emitter located at $\vec{r}_e=1.5\ \mu\text{m}\ \hat{X}$ and observed at a detector located at $\vec{r}_d=-1.5\ \mu\text{m}\ \hat{X}$ (A) with and (B) without Rashba spin-orbit coupling for the same random configuration of scatterers. A scatterer density of 20 scatterers per μm^2 was chosen; each scatterer was modeled as a cylindrical barrier/well of radius 3 nm with the height/depth of the potential randomly chosen between ±.04 eV. The tip was modeled as a hard disc of radius 3 nm. In (A), the amplitude of $\overline{\Delta\mu(\vec{R}_t)}$ is modulated by the Rashba spin-orbit interaction, due to the fact that electrons traveling from the emitter to the detector undergo net spin rotations. In (B), the expected elliptical fringes are observed. The same, arbitrary scale for $\overline{\Delta\mu(\vec{R}_t)}$ was used in both (A) and (B). The following parameters were used in the simulation: $m^*=0.022m_0$, $T=3$ K, $E_F=16$ meV, $\alpha=4\times10^{-11}$ eV m.

$=2n\pi$, the hyperbolic and elliptical modulations are clearly present in Fig. 3(a), along with the circularlike fringes about the emitter and the detector, which leads to a checkered pattern.

For a comparison, simulations were also performed for the same scattering configurations and coupling constants but without the Rashba spin-orbit coupling ($\alpha=0$ eV m). The fermi energy of these simulations E_F' was chosen to be slightly higher in energy than E_F in Fig. 3(a) so that the magnitude of the fermi vectors was the same for both simulations, i.e., $\bar{k}_F'=\bar{k}_F$. As expected, only regular elliptical fringes about the emitter and detector are shown in Fig. 3(b), with any resulting modulation arising from the particular scatterer configuration. Note that the intensities of the fringes are larger when the tip is near to the detector than the corresponding fringes in the presence of Rashba coupling. Figures 4(a) and 4(b) demonstrates this more clearly by plotting a slice of $\Delta\mu(\vec{R}_t)$ [shown in Figs. 3(a) and 3(b)] along the $\hat{Y}$ axis, passing through the detector. Near the detector, the

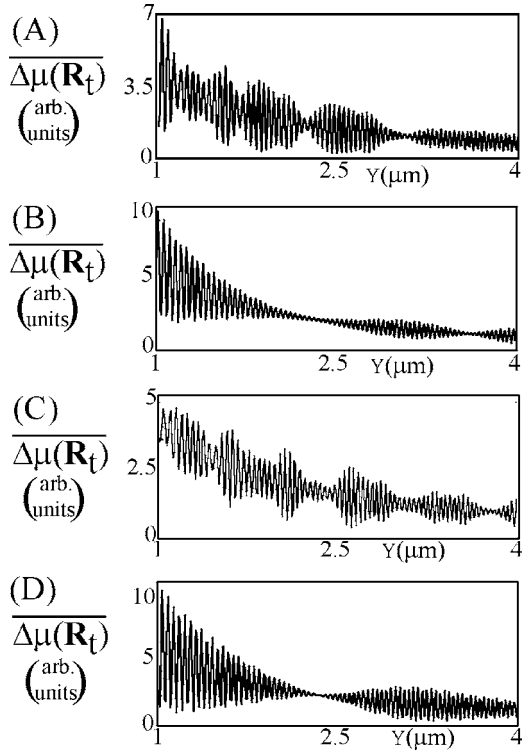

FIG. 4. Slices of $\overline{\Delta\mu(\vec{R}_t)}$ through the detector at $\vec{r}_d=-1.5\ \mu\text{m}\ \hat{X}$. The plots shown in (A) and (B) come from Fig. 3. Modulations are clearly evident in (A) due to spin-orbit coupling. Note also that the intensity of the fringes is larger in the absence of spin-orbit coupling [(B) vs (A)]. However, the fringe intensities also depend upon the configuration of the random impurities. (C) and (D) show the same slice of $\overline{\Delta\mu(\vec{R}_t)}$ for a different configuration of scatterers. Note again that modulations due to Rashba coupling are present in (C) and not in (D).

magnitude of $\overline{\Delta\mu(\vec{R}_t)}$ is greater in the absence of Rashba coupling. However, the magnitudes of $\overline{\Delta\mu(\vec{R}_t)}$ with and without spin-orbit coupling are comparable far away from the detector. This is due to the fact that far away from the detector and emitter, the scattered wave functions can no longer resolve the detector and the emitter, i.e., $\hat{U}(k_\alpha r_{k,d},\theta_d^k)\hat{U}(k_\alpha r_{e,k},\theta_e^k)\approx\hat{1}$, which makes $\Delta\mu(\vec{R}_t)$ independent of α. It must be stressed, however, that although the form of the fringe pattern is robust to scatterer configurations, the overall intensity does depend on the scattering configuration. Figures 4(c) and 4(d) give the same slice through a system with a different set of scatterers.

B. Two scatterer solution

As mentioned earlier, if there is only one QPC, the effects of spin-orbit coupling are not observed if the electron trajectories from and towards the QPC are purely one dimensional. As shown in Fig. 5, two-dimensional multiple-scattering trajectories exist for electrons exiting and arriving at the detector. Consider the case of two scatterers: a moveable scatterer at $\vec{R}_t$ and a fixed scatterer at $\vec{r}_s$. In addition, both the tip and the fixed scatterer will be modeled as being infinite potential

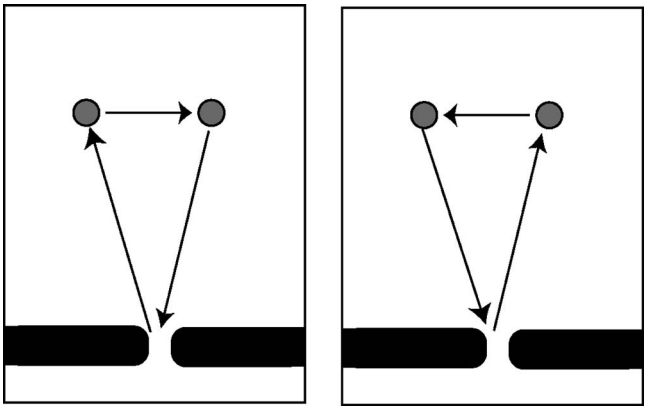

FIG. 5. Possible multiple scattering trajectories which result in a net spin rotation applied to spins which make round trips from the emitter back to the emitter. Since the path is two dimensional, a net spin rotation results, even when the detector and the emitter are the same.

barriers of radius 3 nm. Using Eq. (43), the value of the wave function at each of the two scatterers is given by

$$\Psi(\vec{R}_t) = \lambda_{s,t}\Phi(\vec{R}_t) - \lambda_{s,t}G_0^s(\vec{R}_t)\Phi(\vec{r}_s), \tag{58}$$

$$\Psi(\vec{r}_s) = \lambda_{s,t}\Phi(\vec{r}_s) - \lambda_{s,t}G_0^t(\vec{r}_s)\Phi(\vec{R}_t), \tag{59}$$

where $\lambda_{s,t}=(1-\mathrm{Det}[G_0^t(\vec{r}_s)])^{-1}$. This includes all orders of scattering between the two scatterers (i.e., any number of bounces between the two scatterers). The change in current as a function of $\vec{R}_t$ in the presence of the fixed scatterer at $\vec{r}_s$ and a random configuration of weak scatterers can be found by inserting Eqs. (58) and (59) into Eq. (50) and performing the thermal average using Eq. (52). Since $\bar{t}\ll 1$ in the s-wave limit, it is useful to expand $\Delta\mu(\vec{R}_t)$ in powers of $\bar{t}$. The single scattering contribution has already been discussed, and is given in Eq. (56), which is order $\bar{t}^2$. The next term of order $\bar{t}^3$, which involves the interference between the trajectories shown in Fig. 5 and the single scattering trajectories, can be written as

$$\begin{aligned}\overline{\Delta_{(3)}\mu(\vec{R}_t)} = {} & \exp(i\bar{k}\tilde{R}_S)[K_1(\vec{R}_t)\exp(ik_\alpha\tilde{R}_S) + K_2(\vec{R}_t)\exp(ik_\alpha\tilde{R}_D)] \\ & + \exp(i\bar{k}\tilde{R}_S)[K_3(\vec{R}_t)\exp(-ik_\alpha\tilde{R}_S) \\ & + K_4(\vec{R}_t)\exp(-ik_\alpha\tilde{R}_D)] + \exp(i\bar{k}\tilde{R}_D) \\ & \times[L_1(\vec{R}_t)\exp(ik_\alpha\tilde{R}_S) + L_2(\vec{R}_t)\exp(ik_\alpha\tilde{R}_D)] \\ & + \exp(i\bar{k}\tilde{R}_D)[L_3(\vec{R}_t)\exp(-ik_\alpha\tilde{R}_S) \\ & + L_4(\vec{R}_t)\exp(-ik_\alpha\tilde{R}_D)] + \mathrm{H.c.},\end{aligned} \tag{60}$$

where $\tilde{R}_S=r_{\mathrm{tip},d}+r_{s,\mathrm{tip}}$ and $\tilde{R}_D=r_{\mathrm{tip},d}-r_{s,\mathrm{tip}}$. The functions $K_1(\vec{R}_t)$, $K_2(\vec{R}_t)$, $K_3(\vec{R}_t)$, and $K_4(\vec{R}_t)$ (which mostly represent the interference between the impurity single scattering events and the trajectories shown in Fig. 5) are nonoscillatory functions of $\vec{R}_t$ which depend upon the configuration of random scatterers, whereas the functions $L_1(\vec{R}_t)$, $L_2(\vec{R}_t)$, $L_3(\vec{R}_t)$, and $L_4(\vec{R}_t)$ [which represent the interference between the single scattering trajectories (for the tip and the fixed impurity) and the multiple-scattering trajectories shown in Fig. 5] are nonoscillatory functions of $\vec{R}_t$ which only depend upon the position of the fixed scatterer at $\vec{r}_s$. Figure 6 shows a simulation of $\overline{|\Delta_{(3)}\mu(\vec{R}_t)|}$ in Eq. (60) for a fixed, hard disc scatterer of radius 3 nm located at $\vec{r}_S=1.7\ \mu\mathrm{m}\ \hat{X}+2.4\ \mu\mathrm{m}\ \hat{Y}$. The detector/emitter QPC was placed at $(X,Y)=(0\ \mu\mathrm{m},0\ \mu\mathrm{m})$. Figure 6 represents the evaluation of Eq. (60) for the following parameters: $T=3$ K, $m^*=0.022m_0$, $\alpha=4\times10^{-11}$ eV m, and $E_F=16$ meV (the same parameters as those given in Fig. 3). The random impurities were again modeled as cylindrical wells/barriers of radius 3 nm with depth/height randomly chosen between ±.04 eV and with a scatterer density of 20 scatterers per $\mu\mathrm{m}^2$. Modulations due to spin-orbit coupling are again present, as predicted in Eq. (60).

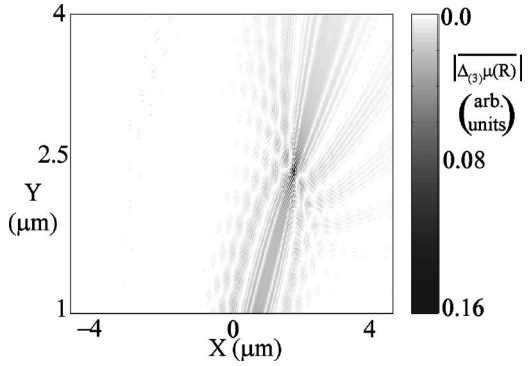

FIG. 6. Calculation of $\overline{|\Delta_{(3)}\mu(\vec{R}_t)|}$ in Eq. (60) for a fixed hard disc scatterer of radius 3 nm located at $\vec{r}_S=1.7\ \mu\mathrm{m}\ \hat{X}+2.4\ \mu\mathrm{m}\ \hat{Y}$. The modulations due to Rashba spin-orbit coupling are seen, similar to those shown in Fig. 3. These modulations mainly result from the interference between the trajectories shown in Fig. 5 and the single scattering trajectories from the tip and fixed scatterer. The flux scale and parameters used in the calculation of $\overline{|\Delta_{(3)}\mu(\vec{R}_t)|}$ are the same as those given in Fig. 3.

If the scattering amplitudes $\bar{t}$ become large, then higher orders (i.e., multiple bounces) must also be included. The interference between these different trajectories can lead to resonances induced by the scattering configuration. For the trajectories shown in Fig. 5, however, no resonances due to spin rotation can be generated, since no net spin rotation is generated if the particle bounces from scatterer A to scatterer B and back to scatterer A again, as shown in Fig. 7(a). The lack of spin rotation for such trajectories can be seen using the exact form of $\hat{G}_0^k(\vec{R})$ given in Eq. (33) as follows:

$$\hat{G}_0^A(\vec{R}_B)\hat{G}_0^B(\vec{R}_A) \propto \hat{1}. \tag{61}$$

However, for three or more scatterers [as shown in Fig. 7(b)], there exist trajectories which will give a net spin rotation. Calculating possible interference effects between multiple scattering trajectories requires using higher partial waves [Eq. (29)] than the simple s-wave scattering models studied mostly in this paper, and will be investigated in the future.

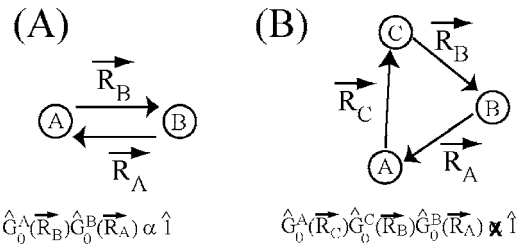

FIG. 7. Possible higher-order scattering processes. For two scatterers shown in (A), if the electron bounces between scatterer A and B, no net spin rotation results. For three or more scatterers, however, net spin rotation can occur. Such a possibility is shown in (B), where an electron traveling from A to C to B to A undergoes a spin rotation.

VI. CONCLUSIONS

In this paper, a partial wave expansion for scattering from a cylindrical potential in the presence of Rashba spin-orbit coupling was developed and was used to construct an operator $\hat{T}_k$ which generates the scattered wave from the incident wave at scatterer k. This allowed for the development of point scattering models beyond the s-wave limit. The often studied s-wave scattering from δ-function potentials are shown to be different from the s-wave models developed in this work due to the fact that cylindrical wells and barriers do not scatter in the δ-function limit; however, both models give the same qualitative results for the flux calculations presented in this work. Although only s waves were discussed herein, extensions to higher partial wave scattering can be readily performed using the formalism developed in this work. Additionally, the operator $\hat{T}_k$ and the calculated Green's function $\hat{G}_{\pm}(\vec{r}_1,\vec{r}_2,E)$ can be used to apply all the scattering theory machinery to study 2DEG confined in a variety of geometries.

The Rashba spin-orbit coupling was shown to generate additional interference fringes in possible electron imaging experiments which were produced using a moveable scanning probe microscope tip. In the single-scattering limit, spin-orbit coupling does not produce any modulation in the observed flux using a single quantum point contact. This is due to the fact that no net spin rotation is generated from effective one-dimensional trajectories which start and end at the same location. If the injected current through a separate quantum point contact is measured instead, interference effects due to Rashba coupling are observed from the various two-dimensional trajectories from the emitter to the detector. This is due to the noncommutation of the resulting spin rotations along the trajectory, which results in spin-orbit-related interference effects. These interference effects are similar to the D'yakonov-Perel' mechanism of spin dephasing observed in electron systems. If multiple-scattering effects are also included, a single quantum point contact can again be used to observe the spin interference caused by the Rashba spin-orbit coupling.

In the future, calculations involving higher partial waves and stronger scattering will be performed in order to look for possible spin resonances resulting from interference between the various multiple scattering trajectories. In addition, more realistic simulations of the scattering induced by a scanning probe microscope tip, requiring other partial waves in addition to the s waves, will be performed. Finally, the multiple-scattering theory presented in this work can also be used to study scattering and polarization profiles generated in quantum wires where phase coherence effects between the scattered waves can now be fully taken into account.

ACKNOWLEDGMENTS

This work was supported at Harvard University by the Nanoscale Science and Engineering Center (NSF Grant No. PHY-0117795), and by NSF Grant No. CHE-0073544.

APPENDIX A: SOLUTION FOR SCATTERING FROM A BARRIER OR WELL

For the problem of the square well/barrier centered about $\vec{r}_k$, Eqs. (20) and (21) require the various $f_l^{\pm}$ and $d_l^{\pm}$ for $|\vec{r}-\vec{r}_k|=a$ to satisfy the following equations:

$$\begin{aligned}
&\lambda_l^{\pm}J_l(k_{\pm}a)+\sqrt{k_1}f_l^{\pm 1}H_l(k_1a)+\sqrt{k_2}f_l^{\pm 2}H_l(k_2a)\\
&\quad=\sqrt{\kappa_1}d_l^{\pm 1}J_l(\kappa_1a)+\sqrt{\kappa_2}d_l^{\pm 2}J_l(\kappa_2a),\\
&\pm\lambda_l^{\pm}J_{l-1}(k_{\pm}a)+\sqrt{k_1}f_l^{\pm 1}H_{l-1}(k_1a)-\sqrt{k_2}f_l^{\pm 2}H_{l-1}(k_2a)\\
&\quad=\sqrt{\kappa_1}d_l^{\pm 1}J_{l-1}(\kappa_1a)-\sqrt{\kappa_2}d_l^{\pm 2}J_{l-1}(\kappa_2a),\\
&\lambda_l^{\pm}k_{\pm}J_l'(k_{\pm}a)+k_1^{3/2}f_l^{\pm 1}H_l'(k_1a)+k_2^{3/2}f_l^{\pm 2}H_l'(k_2a)\\
&\quad=\kappa_1^{3/2}d_l^{\pm 1}J_l'(\kappa_1a)+\kappa_2^{3/2}d_l^{\pm 2}J_l'(\kappa_2a),\\
&\pm k_{\pm}\lambda_l^{\pm}J_{l-1}'(k_{\pm}a)+k_1^{3/2}f_l^{\pm 1}H_{l-1}'(k_1a)-k_2^{3/2}f_l^{\pm 2}H_{l-1}'(k_2a)\\
&\quad=\kappa_1^{3/2}d_l^{\pm 1}J_{l-1}'(\kappa_1a)-\kappa_2^{3/2}d_l^{\pm 2}J_{l-1}'(\kappa_2a),
\end{aligned}\tag{A1}$$

where

$$\lambda_l^{\pm}=2i^l\exp(i\vec{k}_{\pm}\cdot\vec{r}_k)\exp(-il\theta_0).\tag{A2}$$

Using Eq. (A1), the various values for the coefficients $d_l^{\pm 1}$, $d_l^{\pm 2}$, $f_l^{\pm 1}$, and $f_l^{\pm 2}$ can be found. In order to simplify the presentation of the solution to Eq. (A1), the following functions will be introduced to simplify the solutions:

$$\Delta_l(p,q,a)=J_l(pa)J_{l-1}(qa)+J_l(qa)J_{l-1}(pa),$$

$$\Delta\Delta_l(p,q,a)=J_l'(pa)J_{l-1}'(qa)+J_l'(qa)J_{l-1}'(pa),$$

$$g_l^b(p,q,a)=J_{l-1}(qa)H_l(pa)+(-1)^bJ_l(qa)H_{l-1}(pa),$$

$$\begin{aligned}
G_l^b(p,q,r,a)=&\frac{p\Delta_l(q,r,a)}{q\Delta\Delta_l(q,r,a)}[J_{l-1}'(ra)H_l'(pa)\\
&+(-1)^bJ_l'(ra)H_{l-1}'(pa)]-g^b(p,r,a),
\end{aligned}$$

$$F_l^b(k_\pm,q,r,a) = [J_{l-1}(ra)J_l(k_\pm a) \pm (-1)^b J_{l-1}(k_\pm a)J_l(ra)] - \frac{k_\pm \Delta_l(q,r,a)}{q\Delta\Delta_l(q,r,a)}[J'_{l-1}(ra)J'_l(k_\pm a) \pm (-1)^b J'_{l-1}(k_\pm a)J'_l(ra)]. \quad \text{(A3)}$$

The solution to the above equations can be written as

$$f_l^{\pm 1} = \lambda_l^\pm \frac{F_l^2(k_\pm,\kappa_1,\kappa_2,a)G_l^2(k_2,\kappa_2,\kappa_1,a) - F_l^1(k_\pm,\kappa_2,\kappa_1,a)G_l^1(k_2,\kappa_1,\kappa_2,a)}{\sqrt{k_1}[G_l^2(k_1,\kappa_1,\kappa_2,a)G_l^2(k_2,a_2,\kappa_1,a) - G_l^1(k_1,\kappa_2,\kappa_1,a)G_l^1(k_2,\kappa_1,\kappa_2,a)]} = \lambda_l^\pm \frac{\tilde{f}_l^{\pm 1}}{\sqrt{k_1}},$$

$$f_l^{\pm 2} = \lambda_l^\pm \frac{F_l^2(k_\pm,\kappa_1,\kappa_2,a)G_l^1(k_1,\kappa_2,\kappa_1,a) - F_l^1(k_\pm,\kappa_2,\kappa_1,a)G_l^2(k_1,\kappa_1,\kappa_2,a)}{\sqrt{k_2}[G_l^1(k_2,\kappa_1,\kappa_2,a)G_l^1(k_1,a_2,\kappa_1,a) - G_l^2(k_2,\kappa_2,\kappa_1,a)G_l^2(k_1,\kappa_1,\kappa_2,a)]} = \lambda_l^\pm \frac{\tilde{f}_l^{\pm 2}}{\sqrt{k_2}},$$

$$\begin{aligned} d_l^{\pm 1} = {} & \lambda_l^\pm \frac{J_{l-1}(\kappa_2 a)J_l(k_\pm a) \pm J_l(\kappa_2 a)J_{l-1}(k_\pm a)}{\sqrt{\kappa_1}\Delta(\kappa_1,\kappa_2,a)} \\ & + \frac{\lambda_l^\pm}{\Delta(\kappa_1,\kappa_2,a)} \frac{F_l^2(k_\pm,\kappa_1,\kappa_2,a)[g_l^2(k_1,\kappa_2,a)G_l^2(k_2,\kappa_2,\kappa_1,a) - g^1(k_2,\kappa_2)G_l^1(k_1,\kappa_2,\kappa_1,a)]}{\sqrt{\kappa_1}[G_l^2(k_1,\kappa_1,\kappa_2,a)G_l^2(k_2,\kappa_2,\kappa_1,a) - G_l^1(k_1,\kappa_2,\kappa_1,a)G_l^1(k_2,\kappa_1,\kappa_2,a)]} \\ & - \frac{\lambda_l^\pm}{\Delta(\kappa_1,\kappa_2,a)} \frac{F_l^1(k_\pm,\kappa_2,\kappa_1,a)[g_l^2(k_1,\kappa_2,a)G_l^1(k_2,\kappa_1,\kappa_2,a) - g^1(k_2,\kappa_2)G_l^2(k_1,\kappa_1,\kappa_2,a)]}{\sqrt{\kappa_1}[G_l^2(k_1,\kappa_1,\kappa_2,a)G_l^2(k_2,\kappa_2,\kappa_1,a) - G_l^1(k_1,\kappa_2,\kappa_1,a)G_l^1(k_2,\kappa_1,\kappa_2,a)]}, \end{aligned}$$

$$\begin{aligned} d_l^{\pm 2} = {} & \lambda_l^\pm \frac{J_{l-1}(\kappa_1 a)J_l(k_\pm a) \mp J_l(\kappa_1 a)J_{l-1}(k_\pm a)}{\sqrt{\kappa_2}\Delta(\kappa_1,\kappa_2,a)} \\ & + \frac{\lambda_l^\pm}{\Delta(\kappa_1,\kappa_2,a)} \frac{F_l^2(k_\pm,\kappa_1,\kappa_2,a)[g_l^1(k_1,\kappa_1,a)G_l^2(k_2,\kappa_2,\kappa_1,a) + g^2(k_2,\kappa_1)G_l^1(k_1,\kappa_2,\kappa_1,a)]}{\sqrt{\kappa_2}[G_l^2(k_1,\kappa_1,\kappa_2,a)G_l^2(k_2,\kappa_2,\kappa_1,a) - G_l^1(k_1,\kappa_2,\kappa_1,a)G_l^1(k_2,\kappa_1,\kappa_2,a)]} \\ & - \frac{\lambda_l^\pm}{\Delta(\kappa_1,\kappa_2,a)} \frac{F_l^1(k_\pm,\kappa_2,\kappa_1,a)[g_l^1(k_1,\kappa_1,a)G_l^1(k_2,\kappa_1,\kappa_2,a) + g^2(k_2,\kappa_1)G_l^2(k_1,\kappa_1,\kappa_2,a)]}{\sqrt{\kappa_2}[G_l^2(k_1,\kappa_1,\kappa_2,a)G_l^2(k_2,\kappa_2,\kappa_1,a) - G_l^1(k_1,\kappa_2,\kappa_1,a)G_l^1(k_2,\kappa_1,\kappa_2,a)]}. \end{aligned} \quad \text{(A4)}$$

It is useful to consider the limiting case of a hard disc, i.e., $V_0 \to \infty$. In this case,

$$\kappa_1 = \frac{m^*\alpha}{\hbar^2} + i\sqrt{\frac{2m^*|V_0|}{\hbar^2}},$$

$$\kappa_2 = -\frac{m^*\alpha}{\hbar^2} + i\sqrt{\frac{2m^*|V_0|}{\hbar^2}} \quad \text{(A5)}$$

with $|V_0| \to \infty$. In this limit, the coefficients are given by

$$f_l^{\pm 1} = -\frac{\lambda_l^\pm}{\sqrt{k_1}} \frac{J_l(k_\pm a)H_{l-1}(k_2 a) \pm J_{l-1}(k_\pm a)H_l(k_2 a)}{H_l(k_1 a)H_{l-1}(k_2 a) + H_l(k_2 a)H_{l-1}(k_1 a)},$$

$$f_l^{\pm 2} = -\frac{\lambda_l^\pm}{\sqrt{k_2}} \frac{J_l(k_\pm a)H_{l-1}(k_1 a) \mp J_{l-1}(k_\pm a)H_l(k_1 a)}{H_l(k_1 a)H_{l-1}(k_2 a) + H_l(k_2 a)H_{l-1}(k_1 a)}. \quad \text{(A6)}$$

Note also that in the opposite limit of an infinite well, $V_0 \to -\infty$, the expressions for $f_l^{\pm 1}$ and $f_l^{\pm 2}$ are the same as those given in Eq. (A6).

APPENDIX B: CONSTRUCTION OF $\hat{D}_l$

For an arbitrary plane wave state specifed by energy E and with incident momentum vectors making an angle of θ_0 with respect to the $\hat{Y}$ axis,

$$\begin{pmatrix} \Psi^\uparrow(\vec{R}) \\ \Psi_\downarrow(\vec{R}) \end{pmatrix} = \left[\frac{A}{\sqrt{2}} \exp(i\vec{k}_1 \cdot \vec{R}) \begin{pmatrix} 1 \\ \exp(-i\theta_0) \end{pmatrix} + \frac{B}{\sqrt{2}} \exp(i\vec{k}_2 \cdot \vec{R}) \times \begin{pmatrix} 1 \\ -\exp(-i\theta_0) \end{pmatrix} \right] \quad \text{(B1)}$$

an operator $\hat{D}_l$ can be constructed such that

$$\hat{D}_l \begin{pmatrix} \Psi^\uparrow(\vec{R}) \\ \Psi^\downarrow(\vec{R}) \end{pmatrix} = \exp(il\theta_0) \begin{pmatrix} \Psi^\uparrow(\vec{R}) \\ \Psi^\downarrow(\vec{R}) \end{pmatrix}. \quad \text{(B2)}$$

First define the operator $\hat{P}_l$ by

$$\hat{P}_l = \left(\frac{l}{|l|} \frac{\partial}{\partial R_X} - i \frac{\partial}{\partial R_Y} \right)^{|l|} \tag{B3}$$

with $\hat{P}_0 = 1$. Exponential functions of the form $\exp(i\vec{k}\cdot\vec{R})$, where $\vec{k} = k[\cos(\theta_0)\hat{Y} + \sin(\theta_0)\hat{X}]$, are eigenfunctions of $\hat{P}_l$, where

$$\hat{P}_l \exp(i\vec{k}\cdot\vec{R}) = k^{|l|} \exp(il\theta_0)\exp(i\vec{k}\cdot\vec{R}). \tag{B4}$$

The operator $\hat{D}_l$ can be decomposed in terms of the operators $\hat{P}_l$ as follows:

$$\hat{D}_l = \begin{pmatrix} a_l \hat{P}_l & b_l \hat{P}_{l+1} \\ c_l \hat{P}_{l-1} & d_l \hat{P}_l \end{pmatrix}, \tag{B5}$$

where the coefficients a_l, b_l, c_l, and d_l need to be determined. Operating $\hat{D}_l$ on $\Psi(\vec{R})$ in Eq. (B1):

$$\hat{D}_l \begin{pmatrix} \Psi^{\uparrow}(\vec{R}) \\ \Psi^{\downarrow}(\vec{R}) \end{pmatrix} = \frac{A \exp(il\theta_0)\exp(i\vec{k}_1\cdot\vec{R})}{\sqrt{2}} \begin{pmatrix} a_l k_1^{|l|} + b_l k_1^{|l+1|} \\ \exp(-i\theta_0)(c_l k_1^{|l-1|} + d_l k_1^{|l|}) \end{pmatrix} + \frac{B \exp(il\theta_0)\exp(i\vec{k}_2\cdot\vec{R})}{\sqrt{2}} \begin{pmatrix} a_l k_2^{|l|} - b_l k_2^{|l+1|} \\ -\exp(-i\theta_0)(d_l k_2^{|l|} - c_l k_2^{|l-1|}) \end{pmatrix}$$
$$= \exp(il\theta_0) \begin{pmatrix} \Psi^{\uparrow}(\vec{R}) \\ \Psi^{\downarrow}(\vec{R}) \end{pmatrix}. \tag{B6}$$

The various coefficients must therefore satisfy

$$a_l k_1^{|l|} + b_l k_1^{|1+l|} = 1,$$

$$a_l k_2^{|l|} - b_l k_2^{|1+l|} = 1,$$

$$c_l k_1^{|l-1|} + d_l k_1^{|l|} = 1,$$

$$d_l k_2^{|l|} - c_l k_2^{|l-1|} = 1, \tag{B7}$$

which gives

$$a_l = \frac{k_2^{|l+1|} + k_1^{|l+1|}}{k_2^{|l+1|}k_1^{|l|} + k_1^{|l+1|}k_2^{|l|}},$$

$$b_l = \frac{k_2^{|l|} - k_1^{|l|}}{k_2^{|l+1|}k_1^{|l|} + k_1^{|l+1|}k_2^{|l|}},$$

$$c_l = \frac{k_2^{|l|} - k_1^{|l|}}{k_2^{|l-1|}k_1^{|l|} + k_1^{|l-1|}k_2^{|l|}},$$

$$d_l = \frac{k_2^{|l-1|} + k_1^{|l-1|}}{k_2^{|l-1|}k_1^{|l|} + k_1^{|l-1|}k_2^{|l|}}. \tag{B8}$$

For an arbitrary eigenstate of $\hat{H}_0$ [Eq. (3)] with energy E,

$$\begin{pmatrix} \Psi^{\uparrow}(\vec{R}) \\ \Psi^{\downarrow}(\vec{R}) \end{pmatrix} = \int_0^{2\pi} d\theta_0 \left[\frac{\Psi^1(\theta_0)}{\sqrt{2}} e^{\vec{R}\cdot\vec{k}_1(\theta_0)} \begin{pmatrix} 1 \\ \exp(-i\theta_0) \end{pmatrix} + \frac{\Psi^2(\theta_0)}{\sqrt{2}} e^{\vec{R}\cdot\vec{k}_2(\theta_0)} \begin{pmatrix} 1 \\ -\exp(-i\theta_0) \end{pmatrix} \right]$$
$$\equiv \int_0^{2\pi} d\theta_0 \Psi(\theta_0). \tag{B9}$$

Operating $\hat{D}_l$ upon $\Psi(\vec{R})$ gives

$$\hat{D}_l \begin{pmatrix} \Psi^{\uparrow}(\vec{R}) \\ \Psi^{\downarrow}(\vec{R}) \end{pmatrix} = \int_0^{2\pi} d\theta_0 \exp(il\theta_0)\Psi(\theta_0). \tag{B10}$$

APPENDIX C: THE GREEN'S FUNCTION IN THE PRESENCE OF SPIN-ORBIT COUPLING

The Green's function in the presence of Rashba spin-orbit interaction has a simple form in momentum space and can be written as

$$\hat{G}_{\pm}(E) = -\lim_{\epsilon\to 0} \frac{\hat{1}}{\hat{H} - E \pm i\epsilon}$$
$$= -\lim_{\epsilon\to 0} \frac{m^*}{(2\pi\hbar)^2} \int d\vec{k} \frac{|\vec{k}\rangle\langle\vec{k}|}{|\vec{k}|^2 - \frac{2m^*|\vec{k}|\alpha}{\hbar^2} - \frac{2m^*E}{\hbar^2} \pm i\epsilon}$$
$$\times [\hat{1} + \hat{\sigma}_X \cos(\phi_{\vec{k}}) - \hat{\sigma}_Y \sin(\phi_{\vec{k}})]$$
$$-\lim_{\epsilon\to 0} \frac{m^*}{(2\pi\hbar)^2} \int d\vec{k} \frac{|\vec{k}\rangle\langle\vec{k}|}{|\vec{k}|^2 + \frac{2m^*|\vec{k}|\alpha}{\hbar^2} - \frac{2m^*E}{\hbar^2} \pm i\epsilon}$$
$$\times [\hat{1} - \hat{\sigma}_X \cos(\phi_{\vec{k}}) + \hat{\sigma}_Y \sin(\phi_{\vec{k}})], \tag{C1}$$

where $\phi_{\vec{k}}$ is the angle $\vec{k}$ makes with the respect to the $\hat{Y}$ axis. The form of the Green's function in Eq. (C1) has been used in numerous studies of spin dynamics in 2DEGS. The position space representation of the Green's function $\hat{G}_{\pm}(\vec{r}_1,\vec{r}_2,E)=\langle\vec{r}_1|\hat{G}_{\pm}(E)|\vec{r}_2\rangle$, however, has not been used to the best of the authors' knowledge. In the presence of a scattering potential $V(\vec{r})$ the total wave function with energy E is related to $\hat{G}_{\pm}(\vec{r}_1,\vec{r}_2,E)$ and $V(\vec{r})$ by the Lipmann-Schwinger equation

$$\Psi(\vec{R}) = \Phi(\vec{R}) + \int d\vec{r}\hat{G}_{+}(\vec{R},\vec{r},E)V(\vec{r})\Psi(\vec{r}), \tag{C2}$$

where $\Phi(\vec{R})$ would be the wave function in the absence of the scattering potential $V(\vec{r})$.

Before calculating $\hat{G}_{\pm}(\vec{r}_1,\vec{r}_2,E)$, it is worth noting that the Rashba Hamiltonian $\hat{H}_0$ [Eq. (3)] is invariant to combined rotations in spin and space about the $\hat{z}$ axis:

$$\hat{H}_0 = \hat{M}(\theta)\hat{H}_0\hat{M}^{\dagger}(\theta), \tag{C3}$$

$$\hat{M}(\theta) = \exp\left(-i\frac{\theta}{\hbar}\hat{L}_Z\right)\exp\left(-i\frac{\theta}{2}\sigma_Z\right) = \hat{R}(\theta)\hat{Z}(\theta). \tag{C4}$$

Due to the above symmetry, the Green's function is also invariant:

$$\hat{G}_{\pm}(E) = \hat{M}(\theta)\hat{G}_{\pm}(E)\hat{M}^{\dagger}(\theta). \tag{C5}$$

From Eq. (C5), it follows that

$$\langle\vec{r}_1|\hat{G}_{\pm}(E)|\vec{r}_2\rangle = \langle\vec{r}_1|\hat{M}^{\dagger}(\theta)\hat{M}(\theta)\hat{G}_{\pm}(E)\hat{M}^{\dagger}(\theta)\hat{M}(\theta)|\vec{r}_2\rangle = \hat{Z}^{\dagger}(\theta)\langle\hat{R}(\theta)\vec{r}_1|\hat{G}_{\pm}(E)|\hat{R}(\theta)\vec{r}_2\rangle\hat{Z}(\theta). \tag{C6}$$

$\hat{G}_{\pm}(\vec{r}_1,\vec{r}_2,E)$ can be written as

$$\hat{G}_{\pm}(\vec{r}_1,\vec{r}_2,E) = \lim_{\epsilon\to 0}\frac{-m^*}{(2\pi\hbar)^2}\int d\vec{k}\left(\frac{\exp(\vec{k}\cdot\vec{r})\hat{1}}{|\vec{k}|^2+\frac{2m^*\alpha|k|}{\hbar^2}-\frac{2m^*E}{\hbar^2}\pm i\epsilon}+\frac{\exp(\vec{k}\cdot\vec{r})\hat{1}}{|\vec{k}|^2-\frac{2\alpha m^*|k|}{\hbar^2}-\frac{2m^*E}{\hbar^2}\pm i\epsilon}\right)+\exp(\vec{k}\cdot\vec{r})$$
$$\times\left(\frac{\hat{\sigma}_X\cos(\phi_{\vec{k}})-\hat{\sigma}_Y\sin(\phi_{\vec{k}})}{|\vec{k}|^2-\frac{2m^*\alpha|k|}{\hbar^2}-\frac{2m^*E}{\hbar^2}\pm i\epsilon}-\frac{\hat{\sigma}_X\cos(\phi_{\vec{k}})-\hat{\sigma}_Y\sin(\phi_{\vec{k}})}{|\vec{k}|^2+\frac{2\alpha m^*|k|}{\hbar^2}-\frac{2m^*E}{\hbar^2}\pm i\epsilon}\right), \tag{C7}$$

where $\vec{r}=\vec{r}_1-\vec{r}_2$. In evaluating Eq. (C7), it is advantageous to take $\vec{r}$ to be along say the $\hat{Y}$ axis. If $\vec{r}=r[\cos(\theta)\hat{Y}+\sin(\theta)\hat{X}]$, then $\hat{R}(\theta)|\vec{r}\rangle=|r\hat{Y}\rangle$. Therefore, using Eq. (C6), Eq. (C7) can be written as

$$\hat{G}_{\pm}(\vec{r}_1,\vec{r}_2,E) = \lim_{\epsilon\to 0}\frac{-m^*}{(2\pi\hbar)^2}\int_0^{2\pi}d\phi\int_0^{\infty}dk\left(\frac{k\exp[ikr\cos(\phi)]\hat{1}}{(k-k_1\pm i\epsilon)(k+k_2)}+\frac{k\exp[ikr\cos(\phi)]\hat{1}}{(k+k_1)(k-k_2\pm i\epsilon)}\right)$$
$$-k\left(\frac{Z^{\dagger}(\theta)[\hat{\sigma}_X\cos(\phi)-\hat{\sigma}_Y\sin(\phi)]Z(\theta)}{(k-k_1)(k+k_2\pm i\epsilon)}-\frac{Z^{\dagger}(\theta)[\hat{\sigma}_X\cos(\phi)-\hat{\sigma}_Y\sin(\phi)]Z(\theta)}{(k+k_1\pm i\epsilon)(k-k_2)}\right), \tag{C8}$$

where

$$k_1 = \frac{m^*\alpha}{\hbar^2}+\sqrt{\left(\frac{m^*\alpha}{\hbar^2}\right)^2+\frac{2m^*E}{\hbar^2}},$$

$$k_2 = -\frac{m^*\alpha}{\hbar^2}+\sqrt{\left(\frac{m^*\alpha}{\hbar^2}\right)^2+\frac{2m^*E}{\hbar^2}}. \tag{C9}$$

The integrals in Eq. (C8) can be readily evaluated. The term in $\hat{G}_{\pm}(\vec{r}_1,\vec{r}_2,E)$ proportional to the identity matrix is given by

$$\lim_{\epsilon\to 0}\frac{-m^*}{(2\pi\hbar)^2}\int_0^{2\pi}d\phi\int_0^{\infty}dk\left(\frac{k\exp[ikr\cos(\phi)]}{(k-k_1\pm i\epsilon)(k+k_2)}+\frac{k\exp[ikr\cos(\phi)]}{(k+k_1)(k-k_2\pm i\epsilon)}\right)\hat{1}$$
$$=\lim_{\epsilon\to 0}\frac{-m^*}{2\pi\hbar^2}\int_0^{\infty}dk\frac{J_0(kr)}{k_1+k_2}\left(\frac{k_1}{k+k_1}+\frac{k_1}{k-k_1\pm i\epsilon}+\frac{k_2}{k+k_2}+\frac{k_2}{k-k_2\pm i\epsilon}\right)\hat{1}=-\frac{im^*}{2\hbar^2}\left(\frac{k_1}{k_1+k_2}H_0^{\pm}(k_1r)+\frac{k_2}{k_1+k_2}H_0^{\pm}(k_2r)\right)\hat{1} \tag{C10}$$

which is just the weighted average of two free particle Green's function with different wave vectors k_1 and k_2.

Using the following two integrals:

$$\int_0^{2\pi} d\phi \exp[ikr\cos(\phi)]\sin(\phi) = 0,$$

$$\int_0^{2\pi} d\phi \exp[ikr\cos(\phi)]k\cos(\phi) = -i\frac{\partial}{\partial r}\int_0^{2\pi} d\phi \exp[ikr\cos(\phi)] = -i\frac{\partial}{\partial r}2\pi J_0(kr). \tag{C11}$$

The terms in Eq. (C8) proportional to $\hat{\sigma}_X$ and $\hat{\sigma}_Y$ are given by

$$\begin{aligned}
&\lim_{\epsilon\to 0}\frac{-m^*}{(2\pi\hbar)^2}\int_0^{2\pi} d\phi\int_0^{\infty} dk\frac{kZ^\dagger(\theta)[\hat{\sigma}_X\cos(\phi)-\hat{\sigma}_Y\sin(\phi)]Z(\theta)}{(k-k_1)(k+k_2\pm i\epsilon)} - \frac{kZ^\dagger(\theta)[\hat{\sigma}_X\cos(\phi)-\hat{\sigma}_Y\sin(\phi)]Z(\theta)}{(k+k_1\pm i\epsilon)(k-k_2)} \\
&= \lim_{\epsilon\to 0}\frac{m^* i}{2\pi\hbar^2}\hat{Z}^\dagger(\theta)\hat{\sigma}_X\hat{Z}(\theta)\frac{\partial}{\partial r}\int_0^{\infty} dk\frac{J_0(kr)}{k_1+k_2}\left(\frac{1}{k+k_1}+\frac{1}{k-k_1\pm i\epsilon}-\frac{1}{k+k_2}-\frac{1}{k-k_2\pm i\epsilon}\right) \\
&= \frac{-\hat{Z}^\dagger(\theta)\hat{\sigma}_X\hat{Z}(\theta)m^*}{2(k_1+k_2)\hbar^2}\frac{\partial}{\partial r}[H_0^{\pm}(k_1r)-H_0^{\pm}(k_2r)] = \frac{m^*}{2\hbar^2}[\hat{\sigma}_X\cos(\theta)-\hat{\sigma}_Y\sin(\theta)]\left(\frac{k_1}{k_1+k_2}H_1^{\pm}(k_1r)-\frac{k_2}{k_1+k_2}H_1^{\pm}(k_2r)\right).
\end{aligned} \tag{C12}$$

The Green's function $\hat{G}_{\pm}(\vec{r}_1,\vec{r}_2,E)$ can finally be written as

$$\hat{G}_{\pm}(\vec{r}_1,\vec{r}_2,E) = -i\frac{m^*}{2\hbar^2}\frac{k_1}{k_1+k_2}\begin{pmatrix} H_0^{\pm}(k_1r) & iH_1^{\pm}(k_1r)\exp(i\theta) \\ iH_1^{\pm}(k_1r)\exp(-i\theta) & H_0^{\pm}(k_1r)\end{pmatrix} - i\frac{m^*}{2\hbar^2}\frac{k_2}{k_1+k_2}\begin{pmatrix} H_0^{\pm}(k_2r) & -iH_1^{\pm}(k_2r)\exp(i\theta) \\ -iH_1^{\pm}(k_2r)\exp(-i\theta) & H_0^{\pm}(k_2r)\end{pmatrix}. \tag{C13}$$

As noted earlier, $\hat{G}_{\pm}(\vec{r}_1,\vec{r}_2,E)$ is similar in form to the $\hat{G}_0^k(\vec{R})$ operator [Eq. (33)] found in the partial wave scattering analysis given in the text. It is worth pointing out that, as was the case for $\hat{G}_0^k(\vec{R})$, $\hat{G}_{\pm}(\vec{r}_1,\vec{r}_2,E)\hat{G}_{\pm}(\vec{r}_2,\vec{r}_1,E)\propto\hat{1}$, i.e., no net spin rotation is observed when the particle traverses no net distance along a one-dimensional path.

Consider the experiment shown in Fig. 2 for the case when the detector and the emitter are one and the same. With the approximation to $\hat{G}_0^k(\vec{R})$ made in Eq. (39), it was concluded that Rashba spin-orbit coupling does not give rise to modulations in the net current as a function of $\vec{R}_t$ [Eq. (56)]. It is worth pointing out that the conclusion reached by Eq. (56) is valid, even if the approximation in Eq. (39) is not made. Treating the emitter as a point source, the scattered wave function at the detector/emitter is given by Eq. (32):

$$\Psi(\vec{r}_d) = \sum_{k=1}^{N}\hat{G}_0^k(\vec{r}_d)\Psi(\vec{r}_k) = \sum_{k=1}^{N}\hat{G}_0^k(\vec{r}_d)\hat{G}_+(\vec{r}_k,\vec{r}_d,E)\hat{\eta}, \tag{C14}$$

where $\hat{\eta}$ represents the spin state of the injected electron [can be taken to be either $\binom{1}{0}$ or $\binom{0}{1}$ or some linear combination of the two]. It is easy to show, however, that $\hat{G}_0^k(\vec{r}_d)\hat{G}_+(\vec{r}_k,\vec{r}_d,E)$ is not proportional to the identity matrix. For $\bar{k}r_{k,d}\gg 1$, $\hat{G}_0^k(\vec{r}_d)\hat{G}_+(\vec{r}_k,\vec{r}_d,E)$ can be written as

$$\hat{G}_0^k(\vec{r}_d)\hat{G}_+(\vec{r}_k,\vec{r}_d,E) \propto \frac{\exp(i2\bar{k}r_{k,d})}{r_{k,d}} \times\begin{pmatrix} a_k & b_k\exp(i\theta_d^k) \\ b_k\exp(-i\theta_d^k) & a_k\end{pmatrix}, \tag{C15}$$

where

$$\begin{aligned}
a_k &= \sqrt{\frac{k_2}{k_1}}t_{k,0}^1 + \sqrt{\frac{k_1}{k_2}}t_{k,0}^2, \\
b_k &= \sqrt{\frac{k_1}{k_2}}t_{k,0}^2 - \sqrt{\frac{k_2}{k_1}}t_{k,0}^1.
\end{aligned} \tag{C16}$$

Eq. (C15) indicates that the incident spin state, $\hat{\eta}$, is modified after following the effective 1D trajectory [although Eq. (C15) does not represent a spin rotation since it is not unitary]. However, the only distance dependent factor in Eq. (C15) contains $\bar{k}r_{k,d}$ and does not depend upon k_α. Calculations of $\Delta\mu(\vec{R}_t)$ therefore will not possess any modulations which depend upon the Rashba interaction k_α supporting the original conclusions made in Eq. (56).

*Corresponding author. Email address: jwalls@fas.harvard.edu

[1] S. A. Wolf, D. D. Awschalom, R. A. Buhrman, J. M. Daughton, S. von Molnar, M. L. Roukes, A. Y. Chtchelkanova, and D. M. Treger, Science **294**, 1488 (2001).
[2] *Semiconductor Spintronics and Quantum Computation*, edited by D. D. Awschalom, D. Loss, and N. Samarth (Springer-Verlag, New York, 2002).
[3] I. Zutic, J. Fabian, and S. Das Sarma, Rev. Mod. Phys. **76**, 323 (2004).
[4] S. Datta and B. Das, Appl. Phys. Lett. **56**, 665 (1990).
[5] Y. A. Bychkov and E. I. Rashba, J. Phys. C **17**, 6039 (1984).
[6] G. Dresselhaus, Phys. Rev. **100**, 580 (1955).
[7] J. Nitta, T. Akazaki, H. Takayanagi, and T. Enoki, Phys. Rev. Lett. **78**, 1335 (1997).
[8] E. G. Mishchenko, A. V. Shytov, and B. I. Halperin, Phys. Rev. Lett. **93**, 226602 (2004).
[9] A. A. Burkov, A. S. Nunez, and A. H. MacDonald, Phys. Rev. B **70**, 155308 (2004).
[10] J. Schliemann and D. Loss, Phys. Rev. B **68**, 165311 (2003).
[11] J. E. Hirsch, Phys. Rev. Lett. **83**, 1834 (1999).
[12] S. F. Zhang, Phys. Rev. Lett. **85**, 393 (2000).
[13] M. A. Topinka, B. J. LeRoy, R. M. Westervelt, S. E. J. Shaw, R. Fleischmann, E. J. Heller, K. D. Maranowski, and A. C. Gossard, Nature (London) **410**, 183 (2001).
[14] S. E. J. Shaw, R. Fleischmann, and E. J. Heller, cond-mat/0105354, Phys. Rev. Lett. (to be published).
[15] E. N. Bulgakov and A. F. Sadreev, JETP Lett. **73**, 505 (2001).
[16] J. Cserti, A. Csordas, and U. Zulicke, Phys. Rev. B **70**, 233307 (2004).
[17] J. S. Hersch, Ph.D. thesis, Harvard University, 1999, Chap. 6.
[18] J. I. Inoue, G. E. W. Bauer, and L. W. Molenkamp, Phys. Rev. B **67**, 033104 (2003).
[19] M. A. Topinka, B. J. LeRoy, S. E. J. Shaw, E. J. Heller, R. M. Westervelt, K. D. Maranowski, and A. C. Gossard, Science **289**, 2323 (2000).
[20] M. A. Topinka, R. M. Westervelt, and E. J. Heller, Phys. Today **56** (12), 47 (2003).
[21] M. A. Eriksson, R. G. Beck, M. A. Topinka, J. A. Katine, R. M. Westervelt, K. L. Campman, and A. C. Gossard, Superlattices Microstruct. **20**, 435 (1996).
[22] S. E. J. Shaw, Ph.D. thesis, Harvard University, 2002.
[23] G. Metalidis and P. Bruno, cond-mat/0411733 (unpublished).
[24] B. J. LeRoy, A. C. Bleszynski, K. E. Aidala, R. M. Westervelt, A. Kalben, E. J. Heller, S. E. J. Shaw, K. D. Maranowski, and A. C. Gossard, Phys. Rev. Lett. **94**, 126801 (2005).
[25] E.G. Novik, H. Buhmann, and L. W. Molenkamp, Phys. Rev. B **67**, 245302 (2003).
[26] M. Mendoza and P. A. Schulz, Phys. Rev. B **71**, 245303 (2005).
[27] A. Cresti, R. Farchioni, G. Grosso, and G. P. Parravicini, J. Appl. Phys. **94**, 1744 (2003).
[28] J. B. Miller, D. M. Zumbuhl, C. M. Marcus, Y. B. Lyanda-Geller, D. Goldhaber-Gordon, K. Campman, and A. C. Gossard, Phys. Rev. Lett. **90**, 076807 (2003).
[29] E. J. Heller, K. E. Aidala, B. J. LeRoy, A. C. Bleszynski, A. Kalben, R. M. Westervelt, K. D. Maranowski, and A. C. Gossard, Nano Lett. **5**, 1285 (2005).
[30] D. Grundler, Phys. Rev. Lett. **84**, 6074 (2000).
[31] H. van Houten, C. W. J. Beenakker, J. G. Williamson, M. E. I. Broekaart, P. H. M. van Loosdrecht, B. J. van Wees, J. E. Mooij, C. T. Foxon, and J. J. Harris, Phys. Rev. B **39**, 8556 (1989).
[32] L. D. Landau and E. M. Lifshitz, *Statistical Physics I*, 3rd ed. (Butterworth-Heinemann, Oxford, 1999).
[33] M. I. D'yakonov and V. I. Perel', JETP Lett. **13**, 467 (1971).